INFORMATION TO USERS

This manuscript has been reproduced from the microfilm master. UMI films the text directly from the original or copy submitted. Thus, some thesis and dissertation copies are in typewriter face, while others may be from any type of computer printer.

The quality of this reproduction is dependent upon the quality of the copy submitted. Broken or indistinct print, colored or poor quality illustrations and photographs, print bleedthrough, substandard margins, and improper alignment can adversely affect reproduction.

In the unlikely event that the author did not send UMI a complete manuscript and there are missing pages, these will be noted. Also, if unauthorized copyright material had to be removed, a note will indicate the deletion.

Oversize materials (e.g., maps, drawings, charts) are reproduced by sectioning the original, beginning at the upper left-hand corner and continuing from left to right in equal sections with small overlaps.

Photographs included in the original manuscript have been reproduced xerographically in this copy. Higher quality 6" x 9" black and white photographic prints are available for any photographs or illustrations appearing in this copy for an additional charge. Contact UMI directly to order.

Bell & Howell Information and Learning
300 North Zeeb Road, Ann Arbor, MI 48106-1346 USA
800-521-0600

Factors Influencing the Diurnal Temperature Range in the Contiguous United States

by

Imke Durre

A dissertation submitted in partial fulfillment of the

requirements for the degree of

Doctor of Philosophy

University of Washington

2000

Program Authorized to Offer Degree: Department of Atmospheric Sciences

UMI Number: 9995363

Bell & Howell Information and Learning Company
300 North Zeeb Road
P.O. Box 1346
Ann Arbor, MI 48106-1346

Doctoral Dissertation

In presenting this dissertation in partial fulfillment of the requirements for the Doctoral degree at the University of Washington, I agree that the Library shall make its copies freely available for inspection. I further agree that extensive copying of the dissertation is allowable only for scholarly purposes, consistent with "fair use" as prescribed in the U.S. Copyright Law. Requests for copying or reproduction of this dissertation may be referred to Bell and Howell Information and Learning, 300 North Zeeb Road, P.O. Box 1346, Ann Arbor, MI 48106-1346, to whom the author has granted "the right to reproduce and sell (a) copies of the manuscript in microform and/or (b) printed copies of the manuscript made from microform."

Signature 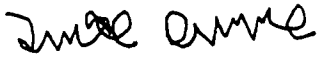

Date September 29th, 2000

University of Washington
Graduate School

This is to certify that I have examined this copy of a doctoral dissertation by

Imke Durre

and have found that it is complete and satisfactory in all respects,

and that any and all revisions required by the final

examining committee have been made.

Chair of Supervisory Committee:

John M. Wallace

John M. Wallace

Reading Committee:

John M. Wallace

John M. Wallace

Conway B. Leovy

Dennis P. Lettenmaier

Date: 9-29-2000

University of Washington

Abstract

Factors Influencing the Diurnal Temperature Range in the Contiguous United States

by Imke Durre

Chairperson of the Supervisory Committee

Professor John M. Wallace
Department of Atmospheric Sciences

During the past several decades, much of the United States has experienced a warming, particularly at night, and a marked decrease in the diurnal temperature range (DTR). Observed variations in many variables have been cited as possible causes of the reported temperature trends. These include increasing cloudiness, rising concentrations of tropospheric aerosols, urbanization and other changes in land cover, ablation of snow cover, and changes in atmospheric circulation patterns. The purpose of this work is to sort out some of the interrelationships among these factors. Through a variety of analyses of historical daily meteorological observations, differences in the effects of cloudiness, land surface conditions, and the atmospheric circulation on daytime versus nighttime temperatures are examined.

It is found that conditions at the land surface have a significant impact on daily maximum temperatures and the DTR. During summer, the tendency for daytime temperatures to be higher when the land surface is dry, which has been well-documented on monthly timescales, is manifested in daily data by a considerable increase in the incidence of near-record high temperatures on days on which the soil is depleted of moisture. In addition, enhanced evapotranspiration associated with the onset and growth of vegetation appears to play a role in the warm season dip of the climatological-mean DTR that is prominent over much of the eastern United States. During winter, snow cover suppresses the DTR under clear skies and reduces the effect of cloudiness on the DTR in the north-central United States.

During the period 1966-1995, the cold season (November-March) DTR decreased over the central and southern United States, but increased over the Northeast, the Pacific Coast, and parts of the interior West. On a national scale, the impact of changes in the sea level pressure field on linear trends in the DTR is found to be small. Thus, much of the long-term trend in the DTR is not linearly related to changes in the atmospheric circulation, but may be attributable either to nonlinear relationships with other changing variables or to anthropogenic factors such as urbanization and the rise in the concentrations of tropospheric aerosols and greenhouse gases.

TABLE OF CONTENTS

LIST OF FIGURES

LIST OF TABLES

ACKNOWLEDGMENTS

I thank my adviser, Dr. John M. Wallace, and the other members of my Supervisory Committee for their guidance and helpful suggestions. My special thanks go to Todd Mitchell and Eric DeWeaver for their assistance in the preparation of figures. I also thank Greg O'Donnell for his assistance in designing and assembling the water balance model used in this study.

This work was supported by the National Science Foundation through the Climate Dynamics Program under Grant ATM-9805886. NCEP/NCAR Reanalysis data were provided by the NOAA-CIRES Climate Diagnostics Center, Boulder, Colorado (http://www.cdc.noaa.gov/).

CHAPTER 1

Introduction

Numerous studies have shown that the diurnal temperature range (DTR), defined as the difference between daily maximum and minimum temperatures, has been decreasing over large portions of the earth's land areas since at least the 1950s (Karl et al. 1984; Balling and Idso 1989; Plantico et al. 1990; Karl et al. 1993b; Lettenmaier et al. 1994; Horton 1995; Easterling et al. 1997; Dai et al. 1999). Ever since Karl et al. (1984) reported a significant downtrend in the DTR over the United States and Canada for the 40-year period ending in 1980, researchers have investigated the possibility that anthropogenic changes in land cover and the concentration of certain atmospheric trace gases and/or particles are responsible for the DTR trend (e.g. Karl et al. 1988; Rind et al. 1989; Karl et al. 1995; Travis and Changnon 1997). However, natural climate variability can also induce variations in the DTR through changes in cloud cover (Karl et al. 1987), soil moisture and vegetation (Cao et al. 1992; Mearns et al. 1995), snow cover (Cerveny and Balling 1992; Karl et al. 1993b), and the atmospheric circulation (Horton 1995; Razuvaev et al. 1995; Easterling et al. 1997). The fact that, in contrast to the global trend, some regions have experienced an increase in the DTR (Karl et al. 1993b; Easterling et al. 1997; Dai et al. 1999) suggests that regional variations in all of these factors should be considered when interpreting DTR trends in the context of anthropogenic climate change.

1.1 Natural Forcings Controlling the Diurnal Temperature Range

The DTR is influenced by diurnally asymmetric forcings, i.e. forcings whose magnitude or sign varies with the time of day. Such forcings can affect the DTR in three ways: they can raise or lower nighttime temperatures while leaving daytime temperatures unchanged, change daytime

temperatures while not affecting nighttime temperatures, or they can simultaneously alter both daytime and nighttime temperatures in such a way that the change in nighttime temperature is opposite in sign to the change in daytime temperature. To first order, latitudinal and seasonal variations in the DTR are driven by variations in insolation. The effect of insolation on the DTR is apparent in the wintertime increase of the DTR towards lower latitudes as well as in the general tendency for the DTR to be larger during the warm season than during the cold season (Robinson et al. 1995; Leathers et al. 1998; Dai et al. 1999). However, this basic picture is strongly modified by other factors.

It is well documented that cloudy days are usually characterized by low DTR, primarily because clouds limit the net radiation at the surface and inhibit the rise of surface air temperature during the day by reflecting solar radiation more efficiently than most surfaces (Karl et al. 1987; Plantico et al. 1990; Robinson 1992; Karl et al. 1993b; Dai et al. 1997, 1999). Clouds also affect surface temperatures by trapping outgoing longwave radiation (Hansen et al. 1995; Mearns et al. 1995; Stenchikov and Robock 1995; Campbell and Vonder Haar 1997). The resulting tendency for nighttime temperatures to be warmer in the presence of clouds than under clear skies has led many scientists to speculate that this mechanism also contributes to a lowering of the DTR by clouds (Karl et al. 1984, 1987; Plantico et al. 1990; Hansen et al. 1995). However, recent theoretical and empirical studies indicate that the magnitude of the longwave cloud forcing exhibits little, if any, variation with time of day (Mearns et al. 1995; Stenchikov and Robock 1995; Campbell and Vonder Haar 1997; Dai et al. 1999; Sun et al. 2000). As a result, clouds are unlikely to significantly influence the DTR through their effect on the longwave radiation balance at the surface. Based on this evidence, it appears that the shortwave cloud forcing is the primary factor contributing to the DTR-cloudiness relationship. However, a more detailed examination of these relationships that includes not only surface humidity, but also tropospheric water vapor, is

warranted. Since the current work focuses on relationships among surface observations, such an analysis is beyond the scope of this study.

The nature and magnitude of the radiative effects of water vapor on the DTR remain a matter of debate. Although atmospheric water vapor contributes significantly to the longwave radiative forcing of daily mean surface air temperature by trapping outgoing longwave radiation, the diurnal variation in this forcing appears to be small (Stenchikov and Robock 1995; Dai et al. 1999). However, it has been speculated that during clear nights, the presence of water vapor, either near the surface or in the free troposphere, may inhibit the formation of surface inversions and thus significantly slow the nighttime drop in surface air temperature. On clear days, the daily maximum temperature should be limited primarily by convective mixing with the overlying atmosphere and should therefore be largely unaffected by the radiative effects of a change in tropospheric water vapor. Thus, even though the contribution of water vapor to the downward flux of infrared radiation may not vary with time of day, its influence on boundary layer processes and surface air temperature may be stronger during clear nights than during clear daytime hours.

Another point of discussion in the literature has been the importance of absorption of near-infrared solar radiation by water vapor. Numerical experiments with radiative-convective models have suggested that the absorption of solar radiation by water vapor may influence daily maximum temperatures and the DTR (Cao et al. 1992; Stenchikov and Robock 1995), but comprehensive analyses of surface and satellite-based observations by Campbell and Vonder Haar (1997) and Dai et al. (1999) provide little evidence of such an effect. In a recent empirical study, Dai et al. (1999) found that under cloud-free conditions, surface specific humidity was slightly more strongly associated with daily minimum temperature than with daily maximum temperature and identified a weak inverse relationship between humidity and the DTR. Judging

from all of these findings and lines of reasoning, it appears that variations in water vapor play a minor role in modulating the DTR in the climatological mean, but may be of greater importance under clear skies.

Surface evapotranspiration, which depends largely on net incoming solar radiation and the amount of moisture available for evaporation, can inhibit the rise in temperature during the day through evaporative cooling of the surface, but has little, if any, effect on nighttime temperatures (Cao et al. 1992; Verdecchia et al. 1994; Mearns et al. 1995; Dai et al. 1999). High evapotranspiration rates from a wet soil imply that the surface latent heat flux is relatively strong, while the sensible heat flux is correspondingly weak. As a result, a large amount of the incoming solar radiation is used for evapotranspiration rather than for surface heating, and daily maximum temperatures are relatively low. Conversely, daytime temperatures can soar to high levels when the soil is dry and evapotranspiration rates are low (Namias 1960; Rind 1982; Shukla and Mintz 1982). Field studies and numerical simulations have also demonstrated that evapotranspiration rates of the soil are higher, and the DTR is lower, over vegetated surfaces than over bare soil (Saltzman and Pollack 1977; Kaufmann 1984; Oliver et al. 1987; Dorman and Sellers 1989; Radersma and de Reider 1996; Schwartz 1996; Xue et al. 1996). Therefore, both a moistening of the soil and the growth of vegetation may act to reduce the DTR relative to dry, bare-soil surface conditions. The relationship between evapotranspiration and temperature has been shown to be strongest during the warm season when insolation and the latent heat flux at the surface are large (e.g. Huang and Van den Dool 1993).

Due to the high albedo of snow, daytime temperatures tend to be lower over snow than over bare ground (Dewey 1977; Walsh et al. 1985; Ruschy et al. 1991; Karl et al. 1993a,b; Leathers et al. 1995; Groisman et al. 1996; Hughes and Robinson 1996; Kalkstein et al. 1996). Snow also limits the heat flux exchange between the soil and the overlying air and thus permits nighttime

surface air temperatures to drop more rapidly than under snow-free conditions (Dewey 1977; Karl et al. 1993b; Leathers et al. 1995). When a sufficient amount of solar radiation reaches the ground, the effect of snow insulating the ground is considerably less important than the albedo effect (Karl et al. 1993b; Leathers et al. 1995). Thus, it appears that the DTR is generally depressed by the presence of snow, but that the magnitude of the depression may vary geographically and seasonally.

In summary, shortwave radiative forcings, which affect mainly daytime temperatures, exert a greater influence on the DTR than longwave radiative forcings, which contribute approximately equally to the variations in daily maximum and minimum temperatures (Stenchikov and Robock 1995; Campbell and Vonder Haar 1997; Dai et al. 1999). Any naturally or anthropogenically driven change in the climate that modifies cloudiness, land surface characteristics, or snow cover extent can also modify the DTR.

1.2 Anthropogenic Forcings of the Diurnal Temperature Range

Human-induced changes in the land cover have been cited as a significant contributor to geographical variations and long-term trends in the DTR. Since buildings and concrete tend to retain heat longer than the natural land surface, urban growth favors a warming of surface air temperatures that is more pronounced at night than during the day (Cayan and Douglas 1984; Karl et al. 1988; Balling and Idso 1989; Gallo et al. 1996, 1999). The resulting decrease in the DTR is believed to be negligible on a continental scale (Karl et al. 1988; Gallo et al. 1999), but may be of greater importance at the regional or local level (Cayan and Douglas 1984; Balling and Idso 1989). On the other hand, the drying of the soil in the interior of continents and the decrease in snow cover which are predicted to occur in conjunction with global warming may lead to regional increases in the DTR (Rind et al. 1989; Cao et al. 1992; Cerveny and Balling 1992).

Human activities may also affect the DTR through an increase in tropospheric aerosols. Aerosols are believed to decrease the amount of solar radiation reaching the surface, both directly by reflecting solar radiation back to space, and indirectly by increasing the number of cloud condensation nuclei in the atmosphere (Charlson et al. 1992). In either case, daytime temperatures and the DTR are expected to be depressed. Although numerical experiments have indicated that both forcings may be significant (Hansen et al. 1995; Stenchikov and Robock 1995), a continental-scale empirical analysis by Karl et al. (1995) only found evidence for a direct radiative forcing of the DTR by aerosols.

The contribution of radiative effects of increased atmospheric CO_2 to the DTR trend remains open to debate (Rind et al. 1989; Cao et al. 1992; Hansen et al. 1995; Stenchikov and Robock 1995; Dai et al. 1999). If CO_2 behaves in the same way as water vapor, then neither the direct longwave and shortwave radiative effects of CO_2 itself nor the CO_2-related water vapor feedback should significantly alter the DTR, although a change in the frequency of near-surface inversions on clear nights in response to increasing CO_2 could conceivably result in higher minimum temperatures and a lower DTR under clear-sky conditions.

1.3 Objectives of This Dissertation

The goal of this work is to compare the contributions of various components of the climate system to the temporal and spatial variability of the DTR in order to facilitate the interpretation of observed DTR trends. The factors considered include cloudiness, soil moisture, vegetation, and snow cover. The impacts of these factors on intraseasonal, interannual, and long-term variations of the daily maximum, minimum, and range of surface air temperature are assessed by means of various analyses of daily surface observations and upper-air fields. In an effort to gauge the

potential contribution of natural climate variability to long-term changes in the DTR, the mechanisms by which changes in the atmospheric circulation can modify the DTR are examined.

Historical daily observations provide the opportunity to either isolate or remove the effects of certain factors by grouping days into various categories. For example, by considering only clear days, the strong influence of cloudiness on the DTR can be removed so as to obtain a clearer picture of the DTR's relationship with other variables. Due in part to limitations in computing resources, relevant studies of the 1980s and early 1990s were limited to using either monthly mean data at a large number of locations or daily observations at a small set of stations. Long records of daily surface observations for a large number of stations are now easily accessible via the Internet. This study will focus on the contiguous United States where stations with high-quality data records are fairly well-distributed.

The following chapters highlight various aspects of relationships between the DTR and other climate factors. Following a description of the data in Chapter 2, Chapter 3 illustrates the association between soil moisture and the occurrence of extreme summertime daily maximum temperatures. In Chapter 4, the seasonal cycle of the diurnal temperature range is examined, with emphasis on the eastern United States where the growth and senescence of vegetation appear to play a role. The influence of cloudiness, snow cover, and the atmospheric circulation on variations and trends of the DTR during the cold season is analyzed in Chapter 5. A summary and concluding remarks follow in Chapter 6.

CHAPTER 2

Data

The data used in this study include daily surface station observations from the First Order Summary of the Day (FSOD) Dataset, selected fields from the NCEP/NCAR Reanalysis Project, various climate indices, and a few miscellaneous datasets. The period of study varies among the analyses, but generally includes 30 to 50 years of data between the 1940s and 1990s.

2.1 Daily Surface Observations

The FSOD dataset available from the National Climatic Data Center (France 2000) provides daily surface observations of sixteen meteorological elements at more than 1500 stations that are either located in the United States or are operated abroad by United States government agencies. The variables used in this study include daily maximum and minimum temperatures (T_{max} and T_{min}), percent of possible sunshine, precipitation, and snow depth. In order to be included in a particular analysis, a station must be located in the contiguous United States and must have "high-quality" records of the variables under investigation. A station's record of a particular variable is considered to be of high quality if measurements are reported on more than 90% of all days within the period of interest. High-quality records of sunshine duration and snow depth are available at fewer stations than high-quality records of temperature and precipitation. As a result, the selection criteria yield different sets of stations for different analyses. Maps showing the locations of the stations used will be presented as appropriate. Among the stations selected, records of temperature, precipitation, and snow depth generally begin in the late 1940s or early 1950s, while reports of sunshine duration do not begin until 1965.

For the purpose of this study, temperatures are converted from integral degrees Fahrenheit to degrees Celsius, retaining the tenths digit; precipitation is converted from hundredths of inches to millimeters, and snow depth is converted from whole inches to centimeters and tenths. For each day and location, the diurnal temperature range (DTR) is calculated by subtracting T_{min} from T_{max}.

The daily percent of possible sunshine is defined as the ratio of observed sunshine duration to the astronomically possible sunshine duration, that is, the time between sunrise and sunset, assuming a smooth spherical earth (Hameed and Pittalwala 1989). Since the 1950s, it has been measured with a photoelectric sunshine recorder whose measurements are adjusted by observers in order to compensate for lack of instrument sensitivity and the effects of complex terrain (Hameed and Pittalwala 1989; Karl and Steurer 1990). Thus, even though changes in observers and observing practices may affect long-term records of the percent of possible sunshine, the observations of this variable appear to be more objective than observers' reports of total cloud amount (Karl and Steurer 1990). Percent of possible sunshine is strongly negatively correlated with total cloud cover (Angell 1990; Karl and Steurer 1990; Plantico et al. 1990) and, therefore, may be viewed as a proxy for total cloudiness.

Observations reported before 1984 underwent a "gross value check" at the National Climatic Data Center (NCDC), while measurements taken since 1984 have been subjected to a more rigorous quality-control and editing procedure (France 2000). During the course of this investigation, the author has identified a few instances in which the reported daily maximum temperature was lower than the daily minimum temperature reported for the same day. In all such cases, both T_{max} and T_{min} were replaced by missing value flags.

The FSOD data have not been corrected for time of observation bias, station moves, instrument changes, or the effects of urbanization. Changes in observation time should have little effect on the results of this study since the vast majority of the stations selected report

observations for the 24-hour period ending at midnight local time. Other inhomogeneities are unlikely to significantly influence the climatological analyses of Chapters 3 and 4. However, due to concerns about the effects of these inhomogeneities on the long-term trends computed in Chapter 5 (Peterson, personal communication), diurnal temperature range trends based on the FSOD data are compared to trends at stations in the Global Historical Climatology Network (GHCN). As described in Peterson and Vose (1997), the monthly-mean maximum and minimum temperature data in the GHCN have been adjusted for discontinuities in time and space and consist mainly of observations from rural stations. From this dataset, 1041 stations that are located in the contiguous United States and have high-quality temperature records have been selected.

2.2 Other Datasets

Among the NCEP/NCAR Reanalysis fields used in this study are daily-mean and monthly-mean geopotential heights (in meters) at the 1000-mb level as well as 00Z and 12Z 850-mb temperatures (in Kelvin) and geopotential heights. The NCEP/NCAR Reanalysis data are assimilated by a state-of-the-art forecast/analysis model at the National Center for Environmental Prediction (NCEP) using observations for the period 1948-1997 (Kalnay et al. 1996). Twice-daily 850-mb temperatures and geopotential heights have been extracted from global four-times daily pressure level data files archived at the NOAA-CIRES Climate Diagnostics Center (CDC). The daily- and monthly-mean fields are produced at the CDC by averaging 00Z and 12Z values from the original fields. All data are provided on a 2.5° × 2.5° latitude/longitude grid. A detailed description of the Reanalysis data and possible sources of error can be found online at http://wesley.wwb.noaa.gov/reanalysis.html as well as in Kalnay et al. (1996).

Additional datasets utilized only in Chapter 3 include observed soil moisture at Peoria, Illinois (Hollinger and Isard 1994), the Palmer Drought Severity Index and Palmer's soil moisture anomaly (Z) Index (Palmer 1965), and the International Soil Reference Information Centre's World Inventory of Soil Emissions Potentials Database (Batjes 1996). These data are described in Section 3.2.

CHAPTER 3

Daily Soil Moisture-Temperature Relationships During Summer

3.1 Background

The summers of 1934, 1936, 1952-54, 1980, and 1988 were characterized by above-normal temperatures, below-normal precipitation, and a deficit in soil moisture over large areas of the central and eastern United States (Diaz 1983; McNab 1989), and many more summers have been marked by more regional drought/heat wave episodes. The tendency for above-normal summertime temperatures to coincide with periods of below-normal precipitation has been illustrated in many empirical studies. During summer, strong negative monthly and seasonal contemporaneous correlations between mean temperature and total precipitation are observed over the southern Great Plains of the United States, and weaker correlations in the same sense are found along the Eastern Seaboard as well as in California, the Pacific Northwest, and the Great Lakes region (Crutcher 1978; Madden and Williams 1978; Namias 1983; Williams 1992; Huang and Van den Dool 1993; Zhao 1993). Tables of regional temperature rankings for the driest ten percent of the summers on record reflect similar geographical variations in the strength of the inverse temperature-precipitation relationship (Karl and Quayle 1981; McNab 1989). While dry summers in New England, the Middle-Atlantic region, and states along the Pacific Coast are about equally likely to have above-median or below-median temperatures, the driest summers in the Southeast are consistently among the warmest on record.

Huang and Van den Dool (1993) have shown that the correlation between precipitation and temperature is significantly larger when precipitation leads temperature by one month than when temperature leads precipitation. Furthermore, both Walsh et al. (1985) and Huang and Van den Dool (1993) found that the inclusion of monthly mean precipitation in addition to monthly mean

temperature improves the prediction of subsequent monthly mean temperature in the interior central and southeastern United States, particularly during the warm season. Over northern Texas, Oklahoma, and Kansas, precipitation alone turned out to be the best predictor in Huang and Van den Dool's analysis. These findings support the widely-held notion that, at least during summer in the interior of continents, surface temperature exhibits a memory of past precipitation.

It has been widely speculated that this memory is provided by the land surface through a positive feedback between soil moisture anomalies and atmospheric anomalies that acts to maintain hot, dry conditions (e.g. Namias 1960; Rind 1982: Shukla and Mintz 1982). According to this hypothesis, a depletion in the amount of water in the soil that is brought about by a deficit in precipitation causes the rate of surface evapotranspiration to decrease. The reduced evapotranspiration is associated with a repartitioning of the surface heat fluxes in favor of the sensible heat flux, which requires a warmer surface and planetary boundary layer. The higher temperatures, in turn, tend to enhance the drying of the soil and lower atmosphere. Additional feedbacks may involve changes in cloudiness, relative humidity, heat capacity, surface albedo, and surface roughness (Bravar and Kavvas 1991; Huang and Van den Dool 1993; Eltahir and Bras 1996).

The strength of the land-atmosphere feedback depends on a number of factors, including the areal extent, magnitude, and persistence of the initial soil moisture anomaly, the strength of the solar forcing, the ratio of potential evapotranspiration to precipitation, the fraction of precipitation recycled from land evapotranspiration, and the strength of the regional dynamical circulation (Delworth and Manabe 1988; Entekhabi et al. 1992; Brubaker et al. 1993; Eltahir and Bras 1996; Fennessy and Shukla 1999; Trenberth 1999). Since air masses tend to lose the oceanic moisture that they carry with them and gain moisture from evapotranspiration as they move inland, the feedback is likely to be strongest in the interior of continents. In addition, the feedback is

expected to operate particularly during summer, when the surface latent heat flux and the fraction of recycled precipitation tend to be large, and the atmospheric circulation is relatively weak.

Evidence in support of the existence of a land-atmosphere feedback comes from numerical experiments as well as from analyses of the relationships between computed indices of soil moisture and observed meteorological conditions. General circulation model simulations of the summer climate in which the initial distribution of soil moisture is varied indicate that a dry soil is associated with low evaporation rates and a warm, dry boundary layer, while a wet soil tends to have the opposite effect (Rind 1982; Shukla and Mintz 1982; Yeh et al. 1984; Yang et al. 1994). Furthermore, the correlations between monthly precipitation and the next month's mean temperature based on multi-year runs of the National Center for Environmental Prediction's Medium-Range Forecast Model resemble the observed correlation pattern over the United States only when the soil moisture in the model is allowed to interact with the atmosphere (Huang and Van den Dool 1993).

For lack of a network of soil moisture observations, empirical studies of soil moisture-temperature relationships have generally employed estimates of soil moisture based on meteorological observations. Early indices of land-surface aridity such as those by Penman (1948), Budyko (1956), and CNC (1959) were based on empirical or semi-empirical relationships between measured evapotranspiration and climate factors, but did not capture the physical processes involved in land-atmosphere interaction. More recently, researchers have attempted to incorporate some of these processes into their aridity indices. Walsh et al. (1985), for example, calculated a soil moisture depth parameter whose time rate of change equals the difference between actual precipitation and computed evapotranspiration. More sophisticated water balance models that include the effects of runoff have been used for the computation of the Palmer Z and Drought Severity Indices (Palmer 1965) as well as in a study by Huang et al. (1996) which

explored the possibility of generating a database of computed monthly soil moisture for the United States. Georgakakos et al. (1995) applied a full-fledged hydrological model with a daily, rather than monthly, time step to two watersheds in the Great Plains in order to study land-atmosphere interaction. All of these methods produce soil moisture proxies that appear to be reasonably consistent with observations of precipitation, runoff, and soil moisture where available.

Studies based on the various soil moisture indices have generally yielded similar soil moisture-temperature relationships. Regardless of the analysis method or soil moisture parameter used, the results for warm-season months indicate that, particularly in inland, non-arid areas, a wet soil tends to depress the concurrent and subsequent monthly mean temperature, while a drier-than-normal soil is favorable for higher-than-expected monthly mean temperatures (Walsh et al. 1985; Karl 1986; Chang and Wallace 1987; Williams 1992). Furthermore, contemporaneous soil moisture-temperature correlations are consistently more strongly negative than correlations between precipitation and temperature (Huang et al. 1996). When predicting monthly mean temperatures, the inclusion of antecedent soil moisture in addition to antecedent temperature can enhance the predictive skill over large portions of the interior United States during the warm season, particularly at lags of several months (Huang et al. 1996). According to Karl (1986), the relatively weak dependence of temperature on antecedent soil moisture anomalies in arid regions such as the Southwest stems from the fact that the magnitude of surface evapotranspiration is low in these areas, even during periods of above-normal precipitation. Due to processes such as stratus clouds, sea breezes, and general onshore advection, which can suppress daytime temperatures (Walsh et al. 1985; Karl 1986), soil moisture tends to also be only weakly associated with subsequent temperature along the Pacific and Atlantic coasts.

Since evapotranspiration takes place primarily during the day, it follows that daytime temperatures should be more sensitive to variations in soil moisture than nighttime temperatures. This hypothesis is supported by the findings of Chang and Wallace (1987), Williams (1992), Georgakakos et al. (1995), and Huang et al. (1996). Using 5-day mean soil moisture time series computed for the Bird Creek, Oklahoma, and Boone River, Iowa, watersheds with a rainfall-runoff-routing model, Georgakakos et al. (1995) showed that, at Bird Creek during summer, the correlation between soil moisture and daily maximum temperature peaks when soil moisture leads maximum temperature by 5-10 days. At Boone River, on the other hand, the highest correlation is found at zero lag. Based on these results it appears that the strength of the local land-atmosphere feedback varies geographically even on the time scale of days. Furthermore, temperature appears to be more sensitive to negative soil moisture anomalies than to positive ones (Georgakakos et al. 1995), indicating that the relationship between soil moisture and temperature may be nonlinear. Williams (1992) noted that the highest recorded temperature in July tends to be higher during dry spells than during wet spells, suggesting that at least the upper part of the distribution of maximum temperatures is shifted towards higher values under dry conditions.

In this chapter, the relationship between soil moisture and the frequency of extreme summertime daily maximum temperatures across the United States are examined in an effort to expand upon the work of Williams (1992), Georgakakos et al. (1995), and Huang et al. (1996). A simple water balance model similar to the one described by Huang et al. is used to compute soil moisture time series from observed precipitation and temperature. As in Huang et al., the use of a simple water balance model in lieu of a more complex rainfall-runoff-routing model such as that employed by Georgakakos et al. is the vehicle for extending the analysis of data from two watersheds to locations across the United States. However, in order to be able to examine local soil moisture-temperature relationships on daily time scales as in Georgakakos et al., the model is

driven by daily station observations rather than by monthly climate division data. Other changes to Huang et al.'s approach include the estimation of potential evapotranspiration by the Priestley-Taylor method (Priestley and Taylor 1972) rather than by Thornthwaite's method, the incorporation of geographically varying soil water capacity, and the implementation of the Variable Infiltration Capacity (VIC) parameterization (Stamm et al. 1994) for the computation of runoff. The model presented here also contains a crude treatment of the effects of snow on the water balance. The time series of daily soil moisture generated by the model are then used to compare the distribution of summertime daily maximum temperatures at 80 stations across the contiguous United States under conditions of anomalously dry and anomalously wet soil. This approach permits the examination of the sensitivity of extreme daytime temperatures to soil moisture variations.

3.2 Data

The data used in this chapter include daily maximum and minimum temperatures (T_{max} and T_{min}), precipitation, and percent of possible sunshine at 80 First Order Summary of the Day (FSOD) stations in the contiguous United States (France 2000), estimated total available water capacities near the stations (Batjes 1996), observed soil moisture at Peoria, Illinois (Hollinger and Isard 1994), and monthly values of the PDSI and soil moisture anomaly (Z) index (Palmer 1965) for the climate divisions in which the chosen stations are located. The period of record examined is January 1948 through December 1995. From the FSOD dataset, which is described in more detail in Section 2.1, stations have been selected on the basis of geographical location and data availability. A map of the station locations is shown in Figure 3.1. The temperature and precipitation observations are used as input time series to the soil moisture model as well as for subsequent analyses.

The water balance model described in the next section requires the specification of the maximum soil water content (W_{max}). For each station analyzed, this parameter is derived from the International Reference Soil Information Centre's World Inventory of Soil Emissions Potentials Database (ISRIC-WISE) which provides estimated ranges of total available water capacity in the top 0-1 m of soil on a global 0.5° × 0.5° latitude/longitude grid (Batjes 1996). In the dataset, water capacities are expressed as equivalent depths and listed as ranges (e.g. 90-150 mm or ≥200 mm). In most cases, W_{max} for a particular station is taken to be equal to the value at the center of the water capacity range given for the land grid point nearest the station. For the ranges ≤90 mm, ≤150 mm, and 200-500 mm, values of 75 mm, 150 mm, and 200 mm are chosen, since they appeared to best fit the geographical distribution of total available water capacities. Although W_{max} lies between 105 and 135 mm at most stations, it ranges from as low as 75 mm to as high as 200 mm. Numerical experiments with the model indicate that the results of subsequent analyses are not very sensitive to maximum soil water content.

Bi-weekly to monthly soil moisture observations at Peoria, Illinois, as well as the PDSI and Z index are used for model verification and consistency checks. The soil moisture observations were taken in eleven layers between the surface and a depth of 2 m with a neutron probe on a bi-weekly to monthly basis as part of the Illinois Climatology Network (Hollinger and Isard 1994). The PDSI and Z indices are part of the Time-Bias Corrected Temperature-Precipitation-Drought Index dataset (National Climatic Data Center 1998). They are derived from monthly mean temperature and precipitation in a multi-step process that begins with the application of a simple bucket model in an effort to estimate the moisture deficit of a region. For further information, the reader is referred to the dataset documentation and Palmer's (1965) report on the procedure for computing these indices.

3.3 Description and Verification of the Water Balance Model

3.3.1 Model Description

A daily time series of soil moisture is derived for each station by means of a simple water balance model with a daily time step. The model is driven by daily temperature and precipitation observed at the station. Locally, the time rate of change in the amount of water (W) in the top layer of the soil is assumed to depend on the amount added by precipitation (P) minus the losses resulting from evapotranspiration (E) and total runoff (R). Thus, the basic equation of the model is:

$$dW/dt = P - E - R \qquad (3.1).$$

As will be described later in this section, precipitation is assumed to consist of rainfall (P_R) and snow melt (M).

$$P = P_R + M \qquad (3.2)$$

In the absence of snow on the ground, evapotranspiration is computed from potential evapotranspiration (E_p) and an evaporation efficiency factor (β).

$$E = \beta \times E_p \qquad (3.3)$$

Following the work of Manabe et al. (1965), evapotranspiration is assumed to occur at the potential rate when the soil is more than 75% saturated and to decrease linearly with soil moisture below this threshold. Thus, β is expressed as

$$\beta = W/W_{max} \qquad \text{for } W/W_{max} < 0.75 \qquad (3.4a)$$

and

$$\beta = 1 \qquad \text{for } W/W_{max} \geq 0.75 \qquad (3.4b)$$

where W_{max} is the maximum soil moisture content. The value of W_{max} for each station is derived from the ISRIC-WISE dataset as described in the previous section.

E_p is calculated according to the Priestley-Taylor method (Priestley and Taylor 1972), setting the Priestley-Taylor parameter α equal to 1.26 and ground heat flux equal to 10% of the net solar radiation at the surface (Kimball et al. 1997). Daily net solar radiation at the surface is expressed as a function of latitude, elevation, day of the year, surface albedo, and diurnal temperature range ($DTR = T_{max} - T_{min}$), following Buffo et al. (1972), Swift (1976), and Bristow and Campbell (1984). The albedo of the ground is fixed at 0.2, a value that is representative of the albedo of bare ground (Robock 1980). In the formula for daily net radiation, the DTR serves as an indicator of the amount of radiation that is attenuated by clouds and other atmospheric constituents.

Runoff is computed using a Variable Infiltration Capacity parameterization (Stamm et al. 1994) that allows for soil moisture drainage during dry periods and sub-grid scale spatial variability in soil moisture capacity. Total runoff is divided into two components, base flow (Q_b) and direct runoff (Q_d):

$$R = Q_b + Q_d \qquad (3.5).$$

Base flow is assumed to be proportional to soil moisture storage:

$$Q_b = k_b \times W \qquad (3.6).$$

Following Stamm et al. (1994), the base flow parameter k_b is fixed at 0.005 day^{-1}. This component of the total runoff ensures that some soil moisture drainage occurs regardless of the amount or type of precipitation.

Direct runoff due to rainfall and snow melt is parameterized as follows (Stamm et al. 1994). Letting I_0 be the initial infiltration capacity of a grid cell, W_0 equal the initial soil moisture content, and I_{max} be the maximum infiltration capacity within the grid cell, the form of the area-

averaged direct runoff depends upon whether or not the sum of I_0 and any rainfall or snow melt on the current day exceeds I_{max}. Thus, Q_d is defined as

$$Q_d = P - W_{max} + W_0 \qquad \text{for } I_0+P \geq I_{max} \qquad (3.7a)$$

and

$$Q_d = P - W_{max} + W_0 + W_{max} \times [1 - ((I_0+P) / I_{max})^{1+B}] \qquad \text{for } I_0+P < I_{max} \qquad (3.7b).$$

Here, B is a shape, or infiltration parameter that is fixed at 0.3, I_{max} is related to W_{max} by the formula

$$I_{max} = W_{max} / (1+B) \qquad (3.8)$$

and I_0 is defined as

$$I_0 = I_{max} \times [1 - (1-A)^{1/B}] \qquad (3.9).$$

The fractional area A of the grid cell with infiltration capacity less than I_0 is given by

$$A = 1 - [(1 - W_0/W_{max})^{B/(1+B)}] \qquad (3.10).$$

Thus, in the presence of precipitation, direct runoff occurs when the soil is saturated as well as under certain conditions when the soil water content is not at its maximum capacity. By definition, Q_d is set to zero when both rainfall and snow melt are equal to zero.

Whenever there is no snow on the ground, the soil moisture is first adjusted for evapotranspiration and base flow, which are based on the previous day's soil moisture. Direct runoff is then calculated from the adjusted soil moisture and the current day's rainfall and snow melt. Finally, the current day's soil moisture is obtained by adding the rainfall and snow melt to the adjusted soil moisture and subtracting the direct runoff (Stamm et al. 1994). Any precipitation that falls when the day's mean temperature (i.e. the average of the day's maximum and minimum temperatures) is below freezing is considered to fall as snow. When snow is on the ground, two

separate water budgets are maintained for the soil and the snow. Both evapotranspiration from the soil and direct runoff are set to zero, while base flow is allowed to continue in accordance with Eq. 3.7. In addition, snow is assumed to sublimate at an estimated potential rate that is derived from the Priestley-Taylor formula by substituting the latent heat of sublimation for the latent heat of vaporization and changing the surface albedo from 0.2 to a value of 0.8 which approximates the albedo of freshly fallen snow (Robock 1980). While the daily mean temperature remains below freezing, the water equivalent of the snow on the ground changes as a result of sublimation and any new snowfall. As soon as the daily mean temperature rises above 0°C, all of the snow is melted, the water equivalent of the melted snow is added to the day's precipitation, and evapotranspiration and direct runoff are allowed to resume. Although this treatment of snow is very crude, it appears to be sufficient for a reasonable simulation of soil moisture during the warm season. Experiments with albedos of 0.15 for bare ground and 0.7 for a snow-covered surface indicate that although soil moisture values are slightly lower when the surface albedo is decreased, soil moisture variability and, therefore, the results of this study are unaffected.

In summary, the model requires latitude, altitude, maximum soil water content, as well as time series of daily maximum temperature, daily minimum temperature, and daily precipitation as input and supplies daily time series of evapotranspiration, base flow, direct runoff, and soil moisture as output. The parameters include the albedos of bare ground and snow, the Priestley-Taylor parameter, the evaporation efficiency factor, the base flow coefficient, and the shape parameter. Using the model, time series of daily soil moisture are calculated for each of the stations shown in Figure 3.1. Since the previous day's soil moisture as well as the current day's average daily temperature and precipitation are essential to the computation of each soil moisture value, the length of the resulting time series at a particular station depends on the length of the

continuous record of precipitation and temperature. At most stations, the time series extend over a period of more than 30 years, and all stations have a continuous record of at least 20 years.

3.3.2 Model Verification

To verify that the daily soil moisture time series generated by the model are realistic, the time series computed for Peoria, Illinois, was compared to soil moisture measurements taken at that site during the common period of record of 1983-1988 (Hollinger and Isard 1994). Experiments with several values of W_{max} and soil moisture observations to various depths indicate that at Peoria, the best agreement between computed and measured soil water content is achieved when observations for the top 0.3 m of soil are considered, and W_{max} in the model is set to 120 mm, i.e. the value at the nearest grid point in the ISRIC-WISE dataset. Using monthly input data and a different water balance model, Huang et al. (1996) found the correlation between observed and simulated soil moisture to be largest for the top 1.3 m of the soil. The time scale of soil moisture variations has been shown to increase with increasing depth (Hollinger and Isard 1994; Georgakakos et al. 1995). One would therefore expect that in order to achieve optimal agreement with the observations, a model with a monthly time step would require a larger maximum soil water content and a deeper soil layer than a model with a daily time step. Thus, the disparity between the results of this study and the results of Huang et al. are consistent with our current understanding of soil moisture variability.

The observed and computed time series for Peoria that exhibit the highest correlation with each other are shown in Figure 3.2a. To facilitate the comparison, computed values (black dots) are plotted only on those dates for which measurements (gray vertical lines) are available. In addition, the means and standard deviations of the two time series as well as the standard error of the model (i.e. the root mean square difference between modeled and observed soil water content)

for December-February, March-May, June-August, and September-November are shown in Table 3.1.

Figure 3.2a and Table 3.1 indicate that the variations in the time series of observed and modeled soil moisture are qualitatively similar. Over the entire six-year period (116 samples), the correlation coefficient between the two time series is 0.86. However, both the mean and standard deviation of W are underestimated by the model in late winter and early spring when snow melt strongly affects soil moisture. During summer, the computed values, on average, are not quite as low as the measurements. Nevertheless, the soil moisture anomalies for May-September of 1983-1988 (48 samples) are correlated at a level of 0.73, and the standard deviations of the modeled and observed time series are nearly identical.

Figure 3.2b displays standardized time series of the observed and computed soil moisture at Peoria, while Figure 3.2c shows the end-of-the-month Z index for the climate division in which Peoria is located. With the annual cycle removed, the correlation between W and observed soil moisture drops to 0.77. The Z index, on the other hand, is correlated with the soil moisture observations at a level of only 0.53. Two factors are likely to be primarily responsible for the difference in the correlations for Z and W. Firstly, Z represents an area average over a climate division, whereas W exhibits variability at one station. Secondly, the use of monthly rather than daily data in the computation of the Z index is likely to introduce errors in the estimation of runoff and evapotranspiration (Alley 1984).

The level of agreement between soil moisture observations and W may vary geographically. Due to the limited availability of long-term soil moisture observations at locations in the contiguous United States, a comparison of observed and computed soil moisture for other stations around the country was not feasible at the time of this study. Nevertheless, the results for Peoria suggest that for the purpose of studying local climatic relationships during the warm season, the

model-calculated soil moisture can be used as a reasonable proxy for the observations.

3.4 Local Soil Moisture-Temperature Relationships

In order to examine the sensitivity of temperatures to low-soil moisture conditions, the summertime (June-August) soil moisture anomalies (W′) at each station are stratified into "low" and "other" values. A day's value of W′ is defined as low if it lies in the bottom quartile of the station's summertime W′ distribution. Figures 3.3 and 3.4 display the distributions of T_{max} and T_{min} for June-August at Little Rock, Arkansas. Each black dot represents a temperature that is observed on a day following a low-W′ day. Since temperatures in the dataset are reported in whole degrees Fahrenheit, this unit of measurement has been retained in the plot. (To prevent the dots from clustering at integer values of temperature and time, the data points have been dispersed into 1°F × 1 day rectangles by adding to each temperature and time a number drawn from a uniform random distribution with a half-width of 0.5.)

Figure 3.3 shows that at Little Rock, hot summer days are more likely during times of low soil moisture than at other times. Of the 1174 observations of $T_{max} \geq 95$°F, 605 (52%) occurred on a day immediately following a low-W′ day. Considering that, by definition, low-W′ days account for only 25 percent of all days, the incidence of such days is about twice as high as would be expected by chance. The fraction of daily maximum temperatures observed on the day following a low-W′ day is even larger for more extreme temperatures: 220 of the 285 days with $T_{max} \geq 100$°F and 34 of the 38 days with $T_{max} \geq 105$°F occurred under low-W′ conditions. In agreement with previous studies (Williams 1992; Georgakakos et al. 1995; Huang et al. 1996), the association between daily minimum temperature and soil moisture anomalies at Little Rock (Fig. 3.4) is much less pronounced than the relationship between T_{max} and W′. In fact, there is little, if

any, separation between the daily minimum temperatures for low-W′ days and other days in Figure 3.4.

An alternative method of presenting the relationship between T_{max} and W′ is to plot the cumulative probability distribution of standardized daily maximum temperatures (T_{max}^{*}) at Little Rock for all summer days (all-day distribution) as well as for low-W′ days (low-W′ distribution; Fig. 3.5). For this purpose, each T_{max} is standardized using the annual cycles of the means and standard deviations of T_{max} as approximated by the first four harmonics of their respective raw climatologies. To derive the distribution for low-W′ days, the percentage of summer low-W′ days that are immediately followed by a day with T_{max}^{*} greater than a certain threshold is calculated for a range of thresholds. The all-day distribution is defined as the distribution of T_{max}^{*} on all summer days (i.e. for all values of W′). To emphasize the difference between the tails of the distributions, the natural logarithm of each probability has been plotted in Figure 3.5. A comparison of the low-W′ and all-day distributions reveals the same relationship between soil moisture and extreme daytime temperatures that is apparent in Figure 3.3: e.g. of all summertime T_{max}, 2.5% are more than two standard deviations above normal, while of the T_{max} on low-W′ days, more than 8% exceed the same threshold.

For an analysis of geographical variations in the strength of the relationship between T_{max} and W′, a "likelihood ratio" (r) has been computed from the low-W′ and all-day percentages of days with T_{max}^{*} above a range of thresholds at each of the 80 stations shown in Figure 3.1. Specifically, for a particular threshold (Σ) and station, r is defined as the ratio of the low-W′ percentage, or conditional probability ($p(T_{max}^{*} > \Sigma \mid \text{low W}')$), to the all-day percentage, or unconditional probability ($p(T_{max}^{*} > \Sigma)$):

$$r(\Sigma) = p(T_{max}^{*} > \Sigma \mid \text{low W}') / p(T_{max}^{*} > \Sigma) \qquad (3.11)$$

The all-day percentage is used in lieu of a percentage derived from the normal distribution since the probabilities at the high end of the all-day distribution tend to be smaller than those at the high end of the normal distribution (Fig. 3.5).

Values of r averaged over stations in eleven geographical regions (Fig. 3.1) are shown in Table 3.2 for $\Sigma = 0$, $\Sigma = 1$, and $\Sigma = 2$. If for a particular region and temperature threshold, the conditional and unconditional probabilities are equal, the corresponding r value is equal to 1.0. On the other hand, when $r(\Sigma = 2)$, for example, reaches a value of 2, then T_{max} is twice as likely to be more than two standard deviations above normal after a low-W′ day as on a randomly selected summer day. Thus, only r values that are considerably larger than one are indicative of a meaningful relationship between T_{max} and W′.

Inspection of Table 3.2 reveals that r tends to decrease as the threshold temperature decreases. For example, at inland stations in the Southeast, r decreases from 3.35 for $\Sigma = 2$ to 1.39 for $\Sigma = 0$. Hence, a prolonged soil moisture deficit has a more pronounced effect on the frequency of very hot days than on the frequency of days with above-normal temperatures. Across the United States, the value of r varies considerably for high temperature thresholds, but is relatively small everywhere for $\Sigma = 0$ (rightmost column in Table 3.2). Overall, the inland portions of the southeastern United States exhibit the largest increase in the frequency of high daytime temperatures between normal- or high-W′ conditions and low-W′ conditions. Among the other inland regions, the probability of observing extremely high T_{max} is also significantly elevated during dry spells in the interior Northeast, Midwest, Great Plains, and Rocky Mountain states. Along the coasts of the Atlantic, the Gulf of Mexico, and the Pacific, $r(\Sigma = 2)$ tends to be somewhat smaller than farther inland. However, this pattern breaks down at lower temperature thresholds. Overall, the weakest relationship between T_{max} and W′ is found along the Pacific Coast, in the Pacific inland region, and in the Southwest.

These geographical differences are in general agreement with those documented by Crutcher (1978), Madden and Williams (1978), Karl and Quayle (1981), Namias (1983), Walsh et al. (1985), Karl (1986), McNab (1989), Williams (1992), Huang and Van den Dool (1993), and Huang et al. (1996). However, for extreme T_{max}, the relationship between T_{max} and W′ is strongest in the Southeast rather than in the Southern Great Plains where correlations of mean temperature with precipitation and soil moisture tend to be largest. It is also interesting to note that Karl and Quayle (1981) and McNab (1989) found dry summers in the Northeast to be equally likely to have above-median and below-median monthly mean temperatures, while this study shows that a relatively large fraction of daily maximum temperatures that are at least two standard deviations above normal occurs under low-soil moisture conditions. This difference is likely to be attributable to the greater dependence of daily maximum temperatures on soil moisture as well as to the nonlinearity inherent in the soil moisture-temperature relationship.

Based on the evidence presented in Table 3.2, the association between T_{max} and W′ appears to be strongest in inland regions that normally experience abundant rainfall and rather weak in areas that receive small amounts of rain. To further examine this relationship, cumulative probability distributions of $T_{max}^{\bullet}$ under low-W′ conditions and the corresponding likelihood ratios have been computed for humid inland, arid inland, and humid coastal stations (Table 3.3). Here, a station is considered to be located inland if it lies at least 150 km from the nearest coastline and to have a humid (dry) climate if it records more than 1000 mm (less than 300 mm) of precipitation annually. This stratification yields groups of 12 humid inland, 14 arid inland, and 8 humid coastal stations. Because, according to these definitions, only one coastal station is classified as arid, no statistics are included for the arid coastal category.

Table 3.3 confirms the impressions gained from Table 3.2. At humid inland stations, the probability of observing a T_{max} that is more than two standard deviations above normal is more

than three times higher following the occurrence of a low-W′ day than on a randomly selected day. Adjacent coastal stations exhibit a 2.4-fold increase in the same probability, while desert and semi-desert locations exhibit only a 1.6-fold increase. As in Table 3.2, these contrasts are less pronounced for less extreme temperature thresholds.

To investigate the temporal persistence of the relationship between T_{max} and W′, $r(\Sigma = 2)$ has been computed for various times between 60 days prior to a low-W′ day (lag N = -60) and 60 days after a low-W′ day (N = +60) by shifting W′ relative to the June-August time series. For example, when the lag is equal to +1 day, then W′ of June 1-August 30 is matched with T_{max}^{*} of June 2-August 31, while for a lag of +60, W′ of April 3-July 2 is paired with T_{max}^{*} for June 2-August 31. Table 3.4 shows values of $r(\Sigma = 2)$ as a function of the lag between W′ and T_{max}^{*} for the same three groups of stations used to construct Table 3.3.

Overall, the r values are relatively symmetric about the zero lag. However, at humid inland stations, the values are slightly higher at lags between +5 and +30 days than at -5 to -30 days. At the arid inland stations, on the other hand, the r values appear to be shifted slightly towards negative lags. With increasing positive lag (i.e. following a low-W′ day), $r(\Sigma = 2)$ decreases at approximately the same rate in each of the three regions. Since, around lag zero, the humid inland stations report the largest r values, the relationship between T_{max} and W′ remains significant for a greater length of time at those stations than in the other two regions. Thus, the regional differences that are very pronounced on day 1 persist to some degree for at least a month after the low-W′ event. In this respect, the results of this study are consistent with those of previous investigations that employed monthly rather than daily data (e.g. Williams 1992; Huang and Van den Dool 1993; Huang et al. 1996).

Table 3.5 shows the autocorrelation functions of T_{max}^{*} as well as cross-correlations between W′ and T_{max}^{*} for the summer season. The cross-correlations are computed by shifting the time

series of five-day averages of W′ backward and forward in time relative to the time series of five-day averages of $T_{max}^{\bullet}$ for June-August. Because slightly different data are used for sampling positive lags than for sampling negative lags, the autocorrelations are not completely symmetric about the zero lag.

In Table 3.5, the strongest soil moisture-temperature relationship is again found at humid inland stations. In contrast to the low-W′ probability distributions and likelihood ratios in Tables 3.2 - 3.4, the cross-correlation functions for arid inland and humid coastal stations do not differ significantly from one another. Furthermore, the cross-correlations peak at lag zero in all three regions and are considerably larger when $T_{max}^{\bullet}$ leads W′ by 5 days (lag = -5) than when W′ leads $T_{max}^{\bullet}$ (lag = +5). The high positive correlations at short negative lags reflect the fact that warm, dry weather tends to deplete soil moisture. Compared to the autocorrelations of $T_{max}^{\bullet}$, the correlations between W′ and $T_{max}^{\bullet}$ are smaller, particularly at lag +5, indicating that on a time scale of days, the persistence of T_{max} is a better predictor of T_{max} than soil moisture. However, previous work by Huang et al. (1996) suggests that a combination of W′ and T_{max} should improve the T_{max} forecast, at least in humid inland regions.

3.5 Summary and Discussion

In a prior study, Georgakakos et al. (1995) showed cross-correlation functions of five-day averages of computed soil moisture anomalies and observed maximum temperature anomalies for the Bird Creek, Oklahoma, and the Boone River, Iowa, watersheds. For the period 1949-1988, they found the correlation at Bird Creek to be -0.65 for soil moisture leading temperature by 5-10 days. When the analysis techniques of this study are applied to stations near Bird Creek for a similar period of record, the highest negative cross-correlations between $T_{max}^{\bullet}$ and W′ occur at lag zero and tend to be somewhat smaller (-0.55) than those found by Georgakakos et al. By lag +5,

the correlations have dropped to below -0.4. The magnitude (-0.4) and lag (0) of the peak correlation in the area of Boone River, on the other hand, agree with Georgakakos et al.'s calculations.

The discrepancy between the results of Section 3.4 and those of Georgakakos et al. (1995) can be attributed to the use of two substantially different models for the computation of soil moisture: in contrast to the highly simplified bucket-like one-layer model of the local water balance used here, Georgakakos et al. employed a more complex hydrological model with a two-layer representation of the soil that is calibrated to runoff and applied to an entire watershed. However, it is currently unclear exactly which processes are responsible for the difference in results.

Synoptic-scale circulation patterns that are favorable for strong daytime heating and a lack of precipitation may contribute to the relationship between soil moisture and T_{max}. For example, if a synoptic situation that produces a dry soil persists, there may be a tendency for the days following a low-W′ day to be unusually sunny, resulting in stronger surface heating and higher daytime temperatures. Figure 3.6 shows the distribution of June-August daily maximum temperatures at Little Rock only on mostly sunny days, with low-W′ days identified by black dots, as in Figure 3.3. A day is defined as mostly sunny if the percent of possible sunshine exceeds 75%. In addition, the cumulative probability distributions of summertime T_{max}^{*} for humid inland stations on various categories of days are listed in Table 3.6.

The clustering of black dots (low-W′ days) toward the top of the temperature range appears to be at least as pronounced in Figure 3.6 as in Figure 3.3, suggesting that differences in cloudiness between low-W′ and other days are not the primary factor accounting for the association between low W′ and high T_{max}. The same conclusion can be drawn when comparing the clear-day and all-day distributions for all humid stations (Table 3.6). Table 3.6 also shows that the change in the

distribution of T_{max}^{*} is smaller following a day with no precipitation than after a low-W′ day, indicating that at humid inland stations, the higher percentages after a low-W′ day are not merely a reflection of the meteorological conditions on the previous day, but also incorporate memory of prior meteorological conditions.

Record and near-record high temperatures are found to be particularly likely during periods of moisture deficit over the interior Southeast. According to Brubaker et al. (1993) and Eltahir and Bras (1996), local evapotranspiration contributes a significant fraction of the moisture available for summertime precipitation over this area. Thus, the strength and relatively long memory of the soil moisture-temperature relationship in the Southeast are consistent with the idea that the impact of the land-atmosphere feedback on regional climate is directly related to the fraction of precipitation recycled from land evaporation (e.g. Delworth and Manabe 1988). Although not explicitly included in the water balance model used here, transpiration from vegetation has also been identified as a significant component of the feedback between land and atmosphere (Shukla and Mintz 1982; Dirmeyer 1994; Yang et al. 1994; Koster and Suarez 1996; Xue et al. 1996), since plant transpiration decreases, and daytime leaf temperatures increase when plants become water-stressed (e.g. Somayao et al. 1980; Gardner et al. 1981).

Since the monthly Palmer Z index and PDSI are widely used as indicators of dry spells, it is interesting to compare the dependence of T_{max} on W′, the Z index, and the PDSI. The comparison is best made by using the end-of-the-month values of W′ since individual values of the Z index and PDSI represent conditions at the end of a month. Using index values for May, June, and July, the cumulative probability distributions of all T_{max}^{*} during the month following a low value of each index are computed (Table 3.7). An index value is considered low if it falls into the bottom quartile of all of the index's May-July values. The resulting distributions can be compared to the monthly distribution of T_{max}^{*} obtained when all Junes, Julys, and Augusts are considered, as well

as to the distribution of T_{max} during the month following a low monthly precipitation anomaly (P′).

The frequency of high afternoon temperatures tends to be considerably larger during a summer month after a low P′, W′, Z index, or PDSI than during all summer months combined. The differences among the distributions based on W′ and the Palmer indices are small compared to the shift in the distribution between overall and dry conditions as measured by any of these three indices. Although the percentages following a low-P′ month are slightly smaller than those following a month with a low W′, Z, or PDSI, the difference between the low-P′ and low-W′ distributions is considerably less pronounced for monthly than for daily data. These results suggest that the processes that contribute to the difference between the no-precipitation and low-W′ distributions for daily data (Table 3.6) operate primarily on time scales shorter than one month. Table 3.7 further indicates that, in terms of capturing the summertime relationship between antecedent moisture conditions and T_{max} in humid inland regions on time scales of one month, W′ is interchangeable with the Z index and the PDSI, and P′ provides nearly as much information as any of the soil moisture indices considered.

In summary, it may be concluded from the results of this study that (1) additional information is gained when relationships between meteorological and land surface conditions are studied with daily, rather than monthly, soil moisture time series; (2) in inland regions east of the Rocky Mountains, and particularly in the Southeast, the distribution of summertime daily maximum temperatures is shifted towards higher temperatures when the soil is dry, and (3) this shift is most pronounced at the high end of the frequency distribution, i.e. for near-record high temperatures. As suggested by Walsh et al. (1985) and Karl (1986), a persistent moisture deficit, low evapotranspiration rates, and marine influences appear to weaken the relationship between soil moisture and extreme daytime temperatures in certain parts of the country. Empirical evidence of

the processes responsible for the geographical variations in the strength of the soil moisture-temperature relationship may be gathered in future work by analyzing soil moisture and meteorological observations available from sources such as the Global Soil Moisture Data Bank (Robock et al. 2000). Alternatively, it may be possible to improve the correspondence between observed soil moisture and soil moisture simulated by the water balance model by adding a second soil layer and varying the evaporation efficiency factor based on vegetation type.

Since variations in soil moisture influence daily maximum temperatures, while leaving daily minimum temperatures largely unaffected, the results of this chapter imply that a dry soil favors a higher diurnal temperature range than a wet soil. This finding is in agreement with the results of an empirical case study by Dai et al. (1999) and numerical experiments by Cao et al. (1992), Verdecchia et al. (1994), and Mearns et al. (1995). The potential impact of land surface processes on the DTR is further considered in the next chapter.

TABLE 3.1 Comparison of observed and modeled soil moisture climatologies at Peoria, Illinois, 1983-1988. Means and standard deviations (STD) of soil water content and the standard error (SE) of the model (i.e. the root mean square difference between the modeled and observed soil water content) are given for the three-month seasons December-February (Winter), March-May (Spring), June-August (Summer), and September-November (Fall). All values are in mm. The number of samples (N) is also listed for each season.

Season	*N*	*Observed*		*Modeled*		*SE*
		Mean	*STD*	*Mean*	*STD*	
Winter	18	112	17	102	12	16
Spring	38	91	38	74	27	18
Summer	37	35	23	43	24	24
Fall	23	69	41	70	29	17

TABLE 3.2 Regional values of the likelihood ratio ($r(\Sigma)$) for various thresholds (Σ) of standardized daily maximum temperature ($T_{max}^{\bullet}$). For each threshold, values are relative to the fraction of all summer days with $T_{max}^{\bullet}$ greater than the threshold. See text for further explanation.

Region	*$R(\Sigma=2)$*	*$r(\Sigma=1)$*	*$r(\Sigma=0)$*
Pacific Coast	1.34	1.24	1.14
Pacific Inland	1.59	1.23	1.08
Southwest	1.37	1.39	1.21
Rocky Mountains	2.54	1.58	1.20
N. Great Plains	2.47	1.69	1.26
S. Great Plains	2.45	2.05	1.39
Gulf Coast	2.86	2.11	1.32
Southeast Inland	3.35	2.35	1.39
Midwest	2.70	1.70	1.23
Northeast Inland	2.63	1.57	1.20
Atlantic Coast	2.21	1.57	1.21

TABLE 3.3 Probability (p, in %) and likelihood ratio (r) for various thresholds (Σ) of standardized daily maximum temperature under low-soil moisture conditions at humid inland, arid inland, and humid coastal stations.

Σ	*Humid inland*		*Arid inland*		*Humid coastal*	
	p	*r*	*p*	*r*	*p*	*r*
2.0	5.1	3.3	1.2	1.6	3.7	2.4
1.0	33.9	2.3	21.7	1.4	25.2	1.8
0.0	72.6	1.4	63.8	1.2	65.7	1.3

TABLE 3.4 Likelihood ratio of observing a daily maximum temperature at least two standard deviations above normal (r(Σ=2)) for selected lags between 60 days before (N = -60) and 60 days after (N = +60) a summertime low-soil moisture day.

N	*Humid inland*	*Arid inland*	*Humid coastal*
-60	1.5	0.8	1.4
-30	1.7	1.1	1.1
-15	2.0	1.4	1.4
-10	2.3	1.4	1.9
-5	2.8	1.5	2.1
-1	3.3	1.7	2.5
0	3.4	1.6	2.6
1	3.3	1.6	2.4
5	2.9	1.4	1.9
10	2.5	1.1	1.8
15	2.2	1.1	1.6
30	1.8	1.3	1.4
60	1.5	1.4	1.1

TABLE 3.5 Cross-correlations ×100 of June-August standardized daily maximum temperature ($T_{max}^{\bullet}$) with itself and soil moisture anomalies (W′) for lags between –60 and +60 days. Correlations are computed from time series of five-day averages and are averaged over humid inland, arid inland, and humid coastal stations. A lag of +N (–N) indicates that the time series in the column heading leads (lags) the JJA $T_{max}^{\bullet}$ by N days.

N	*Humid inland*		*Arid inland*		*Humid coastal*	
	$T_{max}^{\bullet}$	*W′*	$T_{max}^{\bullet}$	*W′*	$T_{max}^{\bullet}$	*W′*
-60	12	-7	6	-2	12	-5
-30	17	-13	5	-6	14	-8
-15	24	-25	8	-14	18	-17
-10	27	-33	15	-22	19	-26
-5	46	-41	35	-34	35	-37
0	100	-47	100	-36	100	-38
5	44	-29	35	-15	34	-17
10	25	-20	14	-9	18	-12
15	21	-17	8	-7	16	-11
30	15	-11	5	-4	13	-9
60	6	-10	4	-5	6	-5

TABLE 3.6 Average cumulative probability distributions of standardized daily maximum temperatures at humid inland stations for various categories of summer days (June 1-August 31). All denotes all summer days; P denotes days preceded by a day without precipitation; W′ denotes days preceded by a day with a low soil moisture anomaly; S denotes all mostly sunny days; W′ S denotes mostly sunny days preceded by a day with a low soil moisture anomaly.

Σ	*All*	*P*	*W′*	*S*	*W′S*
2.0	1.5	2.1	5.1	1.9	7.7
1.0	14.9	19.1	33.8	18.9	44.8
0.0	53.1	61.3	72.6	62.1	82.9

TABLE 3.7 Average cumulative probability distributions of standardized daily maximum temperatures at humid inland stations for various categories of summer months. Distributions are given for all Junes, Julys, and Augusts (All) as well as for the months following a May, June, or July with a low monthly precipitation anomaly (P'), a low end-of-the-month soil moisture anomaly (W'), a low Z index (Z), and a low Palmer Drought Severity Index (PDSI).

Σ	*All*	*P'*	*W'*	*Z*	*PDSI*
2.0	1.5	3.2	3.3	3.4	3.2
1.0	14.8	23.3	24.6	24.2	23.8
0.0	52.8	61.4	62.6	62.3	62.6

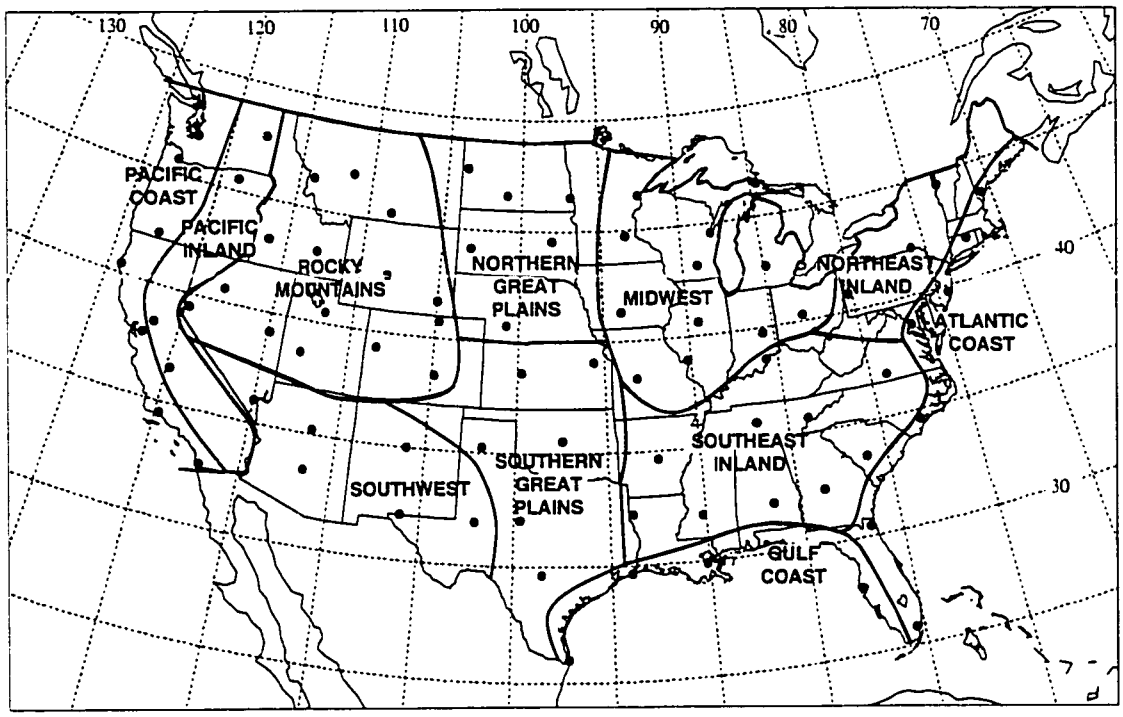

FIGURE 3.1 Map of stations and regions used in this chapter.

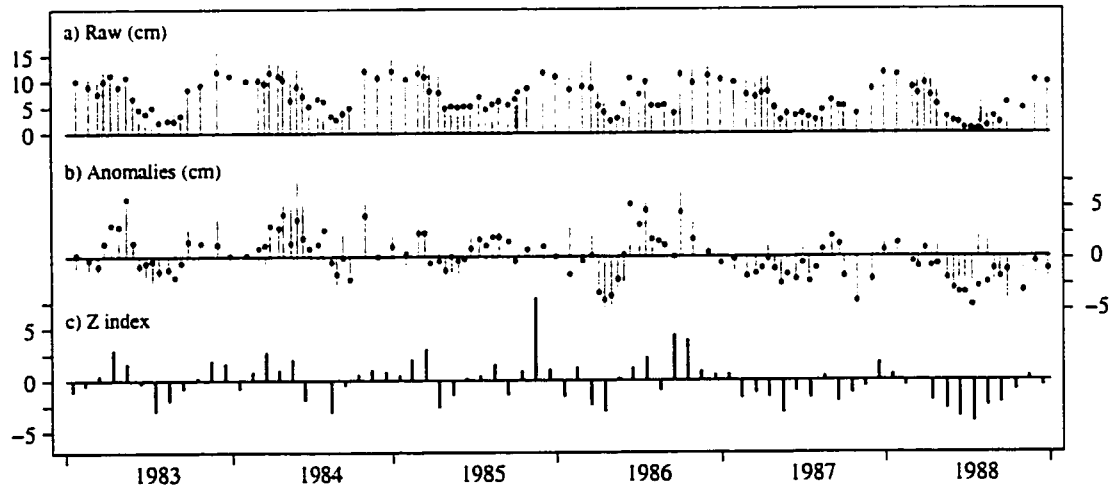

FIGURE 3.2 Soil moisture time series for Peoria, Illinois, 1983-1988. (a) Raw observed and computed soil water content (cm); (b) observed and computed soil moisture anomalies (cm); (c) the Palmer Z index for the climate division of Peoria. In panels a and b, observations are given for the top 30 cm of the soil and are plotted as gray vertical lines. Measurements were taken approximately once a month between October and February and once every two weeks between March and September; three observations are missing. Computed values are identified by black dots and are plotted only on days on which observations are available.

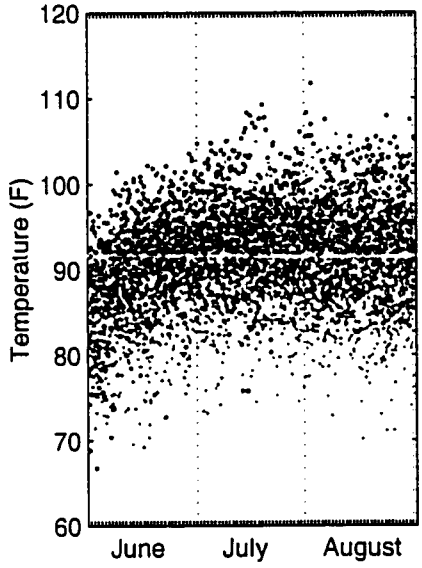

FIGURE 3.3 Distribution of June-August (JJA) daily maximum temperatures at Little Rock, Arkansas, 1949-1995. Calendar days are plotted along the x-axis, temperatures (in °F) along the y-axis. Temperatures observed on the day after a soil moisture anomaly (W') which falls into the lowest quartile of all of the stations' JJA W' values are shown in black.

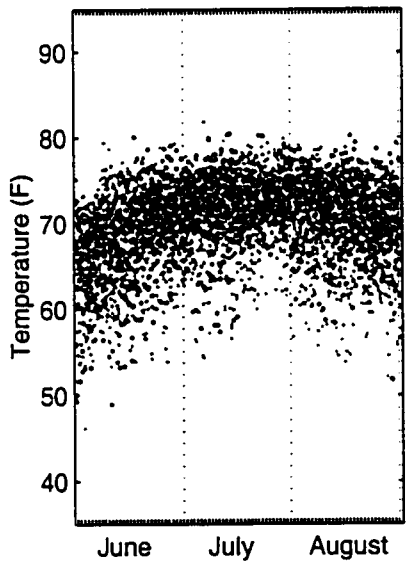

FIGURE 3.4 Distribution of June-August daily minimum temperatures at Little Rock, Arkansas, 1949-1995. Plotting conventions are the same as in Figure 3.3.

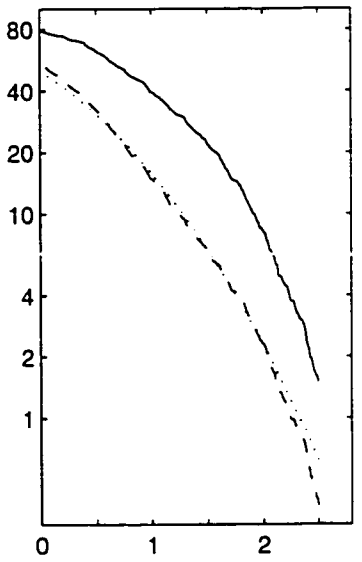

FIGURE 3.5 Cumulative probability distributions of standardized daily maximum temperatures (T_{max}^*). Distributions are based on summer low-soil moisture days (solid line), all summer days (dashed line), and the assumption that T_{max}^* follows a normal distribution (dotted line). Thresholds are plotted on the abscissa; the percentage of T_{max}^* greater than a given threshold are plotted on a logarithmic scale on the ordinate.

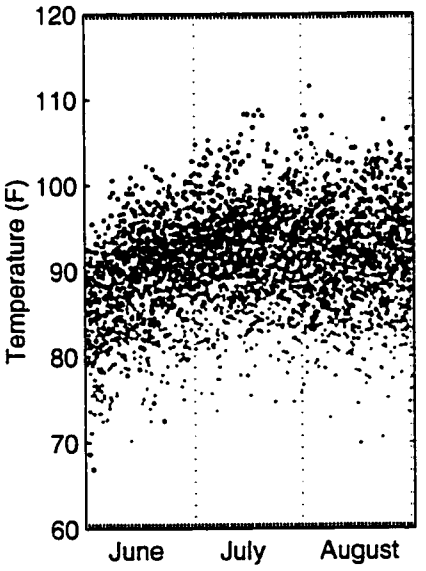

FIGURE 3.6 Distribution of daily maximum temperatures on summer days with more than 75% of possible sunshine at Little Rock, Arkansas, 1949-1995. Plotting conventions are the same as in Figure 3.3.

CHAPTER 4

The Warm Season Dip in the Diurnal Temperature Range Over the Eastern United States

4.1 Background

In recent years, Robinson et al. (1995) and Leathers et al. (1998) have demonstrated that the shape of the annual cycle of the diurnal temperature range (DTR) varies across the contiguous United States. Over much of the West as well as the northern tier states (regions 1 and 3 in Leathers et al.), the DTR peaks during summer and reaches its minimum during the winter. From the central and southern Great Plains eastward to the Atlantic Ocean (region 2 in Leathers et al.), however, the DTR climatology exhibits two comparable maxima, one during spring and one during autumn, that are separated by a distinct, broad summer minimum. The characteristic double peak is not well-simulated by general circulation models: between spring and autumn, the seasonal variations in the DTR tend to be smaller in the models than in the observations (Kukla et al. 1995; Mearns et al. 1995). In light of the widespread decrease in the DTR over the past several decades and its possible relationship to human activities (e.g. Karl et al. 1993b), the correct simulation of the DTR by climate models is of major importance.

An understanding of the reasons for the discrepancy between models and observations may be gained by examining the factors that influence seasonal changes in the DTR. As discussed in Chapter 1, shortwave radiative forcings tend to exhibit a greater diurnal asymmetry than longwave forcings, primarily because the diurnal cycle of solar radiation is considerably more pronounced than the diurnal cycle of thermal radiation (Stenchikov and Robock 1995; Campbell and Vonder Haar 1997; Dai et al. 1999). Factors that may affect seasonal changes in the DTR by

modulating daily maximum temperature include insolation, the reflection of solar radiation by clouds, surface albedo, and surface evapotranspiration (Ruschy et al. 1991; Karl et al. 1993b; Mearns et al. 1995).

The rise in the climatological-mean diurnal temperature range from winter to spring that takes place over most of the United States has been attributed to a decrease in surface albedo as a result of the disappearance of snow cover (Ruschy et al. 1991; Schwartz 1996), an increase in net incoming solar radiation (Ruschy et al. 1991), as well as a lifting of ceiling heights and a decrease in the percentage of coverage of clouds (Karl et al. 1993b). All of these changes enhance the amount of radiation absorbed at the surface during the day and thus favor a more rapid rise in daily maximum temperature than in daily minimum temperature. In much of the northern and western United States, daytime temperatures and the DTR continue to climb up to their summer peak as cloudiness continues to decrease (Leathers et al. 1998). The abrupt leveling off of the DTR after the spring peak in the eastern United States, which occurs despite a continued increase in net radiation and decrease in cloudiness (Ruschy et al. 1991), has been linked to the seasonal onset of the growing season.

Schwartz and Karl (1990), Schwartz (1992), and Schwartz (1996) analyzed changes in the atmospheric boundary layer relative to observed first-leaf emergence dates for cloned species of lilac at stations across eastern North America. According to these studies, atmospheric water vapor increases following the first-leaf date, and the rise in the daily maximum surface air temperature slows relative to the rise in 850-700 mb thickness. The authors conclude that the increase in atmospheric humidity may reflect an enhancement of surface evapotranspiration rates as a result of the onset of foliage production, and that the increase in the surface latent heat flux, in turn, suppresses daytime temperatures and the DTR.

According to Dai et al. (1999), who investigated the observed relationships between the DTR, specific humidity, and soil moisture on clear summer and autumn days, evaporative cooling has a greater influence on the DTR than any direct radiative effects of atmospheric water vapor. Since transpiration rates tend to rise with increasing net incoming solar radiation, and both moisture and vegetation are abundant in the eastern United States during summer, the importance of this effect may be expected to increase until mid-summer and then decrease during late summer and autumn, particularly after the senescence of vegetation (Xue et al. 1996). Evapotranspiration rates are lower and vegetation is less abundant over the western United States than in the East. Therefore, the impact of surface evapotranspiration on the annual march of the DTR is likely to be less important in the West.

In this chapter, daily surface and 850-mb data over the eastern United States are analyzed in search of further evidence of the influence of transpiration from vegetation on seasonal variations in the DTR. The strategy is to (1) examine the distance between the spring and fall peaks in DTR climatologies for various latitude bands in relation to the length of the growing season, (2) determine whether atmospheric changes around the time of the autumn DTR peak mirror those observed during spring, and (3) stratify the data according to the percent of possible sunshine in order to separate the influence of cloudiness on the DTR from other effects. In an attempt to separate the potential effects of surface and boundary-layer processes on surface air temperature from the effects of dynamics in the free atmosphere, a "relative surface air temperature" has been defined. The day-to-day variability of this temperature represents changes in surface air temperature relative to those expected from variations in 850-mb temperatures and, therefore, mainly reflects variability associated with surface and boundary layer processes. The consideration of changes in meteorological conditions around the time of both the spring and fall

peaks in the DTR may permit the extension of Schwartz's findings to include the effects of vegetation on the DTR throughout the growing season.

4.2 Data

The data used in this analysis consist of daily maximum temperature, daily minimum temperature, and percent of possible sunshine at selected First Order Summary of the Day stations across a large portion of the eastern United States (France 2000) as well as 00Z and 12Z 850-mb temperatures and geopotential heights from the NCEP/NCAR Reanalysis (Kalnay et al. 1996). For further details on these datasets, the reader is referred to Chapter 2. Stations whose record of daily maximum and minimum temperatures between 1966 and 1995 is at least 90% complete and which lie within the area of the eastern United States in which the DTR climatology exhibits the characteristic warm season dip are included. In addition, the area of study is adjusted to match the resolution of the NCEP data. The result is a set of 53 stations within the area 31.25°N - 43.75°N, 80°W - 90°W (Fig. 4.1). When analyses are restricted to mostly sunny days, only the 22 stations whose 1966-1995 record of percent of possible sunshine is at least 90% complete are used. These stations are identified by open circles in Figure 4.1.

In an attempt to emphasize variations that may be caused by fluctuations in surface processes, time series of "relative surface air temperature" have been computed for the late afternoon and early morning from daily maximum and minimum surface air temperatures at each station together with 00Z and 12Z 850-mb temperatures and geopotential heights at the nearest NCEP Reanalysis grid point. For each record, the 850-mb temperature (T_{850}) is projected onto the surface by adding to it the product of the dry adiabatic lapse rate ($\Gamma_d = 9.8 \times 10^{-3}$ °C m^{-1}) and the 850-mb level's height (z_{850}) above the surface (z_s). The resulting reference temperature is then subtracted from the corresponding observed surface air temperature to obtain the relative surface

air temperature (T_r). Morning T_r (T_r(am)) is derived from daily minimum temperature (T_{min}) and the same day's 12Z 850-mb temperature and height, while afternoon T_r (T_r(pm)) is derived from daily maximum temperature (T_{max}) and the corresponding 00Z 850-mb data.

$$\begin{aligned} T_r(\text{am}) &= T_{min} - [T_{850}(12Z) + \Gamma_d \times (z_{850}(12Z) - z_s)] \\ T_r(\text{pm}) &= T_{max} - [T_{850}(00Z) + \Gamma_d \times (z_{850}(00Z) - z_s)] \end{aligned} \tag{4.1}$$

Positive (negative) values of T_r indicate that the lapse rate between the surface and the 850-mb level is steeper (less steep) than the dry adiabatic lapse rate. An increase (decrease) in T_r therefore represents either a warming (cooling) of the surface relative to the atmospheric boundary layer or a cooling (warming) of the 850-mb level relative to the surface. As discussed in the previous section, enhanced surface evapotranspiration rates, for example, would act to decrease T_r(pm) by inhibiting daytime surface heating, while leaving T_r(am) unchanged. Any potential differential radiative effects of clouds at the surface and 850-mb level will be minimized by restricting the analysis of T_r to mostly clear days. Differences in temperature advection at the two levels, which may be significant in certain synoptic situations, are likely to average out in the climatological mean.

4.3 Results and Discussion

Figure 4.2 shows the climatologies of the DTR between 80°W and 90°W for five adjacent latitude bands centered at 42.5°N, 40.0°N, 37.5°N, 35.0°N, and 32.5°N. The climatological mean for each station is determined by computing, for each day of the year, the arithmetic mean of the differences between daily maximum and minimum temperatures. The resulting daily means are then averaged over the stations located within each of the five areas. Progressing from north to south, the character of the annual cycle of the DTR clearly changes: the distance between the two

peaks widens during the warm half of the year, the summer dip becomes more pronounced, and the winter minimum becomes less prominent. In the northern two latitude bands, the spring maximum is larger than the autumn maximum, whereas the maxima are of comparable magnitude farther to the south. Based on the findings of the studies cited in Section 4.1, the factors that may contribute to these seasonal and geographical variations in the DTR include net incoming solar radiation at the top of the atmosphere, cloudiness, and evapotranspiration from soil and vegetation.

All other things being equal, an increase in both daily net incoming solar radiation and the length of the day results in enhanced daytime surface heating, while a shortening of the night favors a reduction in radiative cooling and, therefore, a rise in daily minimum temperature. The former effect tends to outweigh the latter (e.g. Ruschy et al. 1991). Thus, based on seasonal changes in net incoming solar radiation and the number of daylight hours alone, one would expect the DTR to be at a minimum in winter and at a maximum in summer, and the amplitude of this seasonal cycle to decrease from north to south. Indeed, the wintertime DTR values tend to be larger in the south than in the north, whereas the summertime values do not increase towards the south. However, the largest values of the DTR are not observed around the time of the summer solstice.

The annual cycle of net shortwave radiation at the surface is modulated by changes in cloudiness. Figure 4.3 shows the climatology of the percent of possible sunshine (p_{sun}) for the 2.5°-wide latitude bands centered at 40°N and 35°N which are representative of the northern and southern portions of the study area. Each climatology constitutes an average over seven stations. While both curves in Fig. 4.3 exhibit a minimum during winter, the amplitude of the seasonal cycle and timing of the maximum in the two regions differ. The annual march is more pronounced in the north, mainly due to lower winter values. The curve of p_{sun} reaches its

maximum during summer in the 40°N latitude band, but remains nearly flat between April and October in the 35°N latitude band. These results are in agreement with published seasonal mean climatologies of total cloud amount and sunshine duration over the eastern United States (Warren et al. 1986; Angell 1990).

A comparison of the shapes of the p_{sun} curves in Figure 4.3 and the corresponding DTR climatologies, plotted as the second and fourth curves from the top in Figure 4.2, reveals a strong correspondence between seasonal variations of the two variables during the cold season. During the warm season, however, the shapes of the p_{sun} and DTR curves differ significantly, indicating that cloudiness cannot be the decisive factor in determining the DTR during that half of the year. To further facilitate the assessment of the effects of seasonal changes in cloudiness on the DTR, the DTR climatologies for mostly sunny days (p_{sun} >75%) and all other days (p_{sun} ≤75%) have been plotted for the 40°N and 35°N latitude bands in Figure 4.4. The climatologies for mostly sunny days, denoted by black dots, are computed by averaging, for each day of the year, only the DTR values that occur on days with p_{sun} >75%.

Except on a few days during December and January in the 40°N latitude band, the average DTR is clearly higher on mostly sunny days than on other days. This difference reflects the efficiency with which clouds inhibit the daytime rise of surface air temperature by reducing the amount of shortwave radiation that reaches the surface. As discussed in Chapter 5, the relatively small effect of cloudiness on the DTR during mid-winter in the north is likely to be in part a result of relatively low incoming solar radiation (Dai et al. 1999) and may also be related to the frequent presence of snow cover (Groisman et al. 1994; Sun et al. 2000). Since the amount of wintertime incoming solar radiation is larger and snow cover is less frequent in the southern region, cloudiness has a stronger influence on the DTR there.

Overall, the characteristic seasonal maxima and minima in the DTR are more pronounced in the climatologies for mostly sunny days than in the other-day climatologies. If changes in cloudiness were responsible for the warm season dip in the DTR, then the amplitude of this dip should be reduced, if not eliminated, in the sunny-day DTR climatology. Instead, the dip is more prominent for p_{sun} >75% (Fig. 4.4, black) than for all days (Fig. 4.2) and is virtually absent when only days with p_{sun} ≤75% are considered (Fig. 4.4, gray). Furthermore, the dip remains prominent even when the DTR climatology is calculated using days on which p_{sun} exceeds 99% (not shown). Together, these results indicate that although cloudiness plays a significant role in determining the DTR on a day-to-day basis within a particular season (Karl et al. 1987; Dai et al. 1999), it does not account for the peculiar character of the annual march of the DTR in the eastern United States. This conclusion is in agreement with Leathers et al.'s (1998) finding that cloud amount does not explain a significant portion of the variance in the DTR's annual march.

The pronounced warm season dip in the sunny-day DTR climatologies further suggests that this dip is caused by a process that limits the ability of solar radiation to heat the surface during the day and whose effect is particularly strong during summer. The north-to-south progression of the climatological peaks in the DTR towards earlier in the spring and later in the fall (Fig. 4.2) is consistent with a lengthening of the growing season from north to south. In order to obtain a more quantitative measure of the change in the warm season inter-peak distance, the dates of occurrence of the spring and autumn maxima at each station are computed from DTR climatologies that have been smoothed with a five-day running mean. These dates are then averaged over each of the five latitude bands, and the difference between the autumn and spring dates is determined. The results, shown in Table 4.1, confirm the impression gained from Figure 4.2. As the spring peak moves from late May in the north to mid-April in the south, the autumn peak shifts from late September to early November, and the inter-peak difference increases from

four months (124 days) to nearly seven months (203 days). Similar results are obtained when the same analysis is conducted for sunny-day DTR climatologies (not shown), again indicating that the timing of the peaks is independent of variations in cloudiness.

A map of 30-year average first-leaf emergence dates of three cloned species of lilac and honeysuckle over a portion of eastern North America (Eastern North America Phenology Network 1999) shows a north-to-south change similar to that of the DTR's spring maximum. The first-leaf date shifts from late April in northern New England to early March in Tennessee and North Carolina. Since lilac and honeysuckle tend to be among the first plants to leaf out, the bulk of the leaves of all plants will probably not emerge until somewhat later. Thus, the timing of the DTR's spring maximum (Table 4.1) appears to be tied to the onset of the growing season. This association is consistent with Schwartz's hypothesis that increased evapotranspiration at the time of green-up may suppress the DTR through daytime evaporative cooling at the surface and may thus contribute to the change in slope of the DTR climatology during spring.

In Figure 4.5, climatologies of average daily maximum and minimum temperature (T_{max} and T_{min}) as well as afternoon and morning relative surface air temperature (T_r(pm) and T_r(am)) on mostly sunny days (p_{sun} >75%) are displayed together with the sunny-day climatologies of the DTR and the daily range of relative surface air temperature. The elimination of days with p_{sun} ≤75% again minimizes the potential effects of variations in cloudiness on the plotted variables. For this figure, values have been averaged over all 22 stations within the study area for which sufficient sunshine data are available. Solid vertical lines mark the dates of the DTR maxima in the annual march. The time rate of change of relative surface air temperature with calendar date, as defined in the previous section, indicates whether the surface is growing warmer or cooler relative to the 850-mb temperature and thus emphasizes the changes in surface air temperature that are due to variations in surface processes. Since, in the climatological mean, diurnal

variations in 850-mb temperature are small, the annual cycles of DTR and the diurnal range in T_r are virtually identical (Fig. 4.5a, c).

On mostly sunny days in spring, T_{max} and T_r(pm) increase rapidly with calendar date leading up to the DTR maximum (Fig. 4.5b, d). The slope in T_r(pm) begins to decrease at or just before the spring DTR peak, and the curve flattens out a few weeks later, whereas T_{max} increases steadily throughout the spring. These results imply that after the DTR maximum, the seasonal warming of the surface relative to the warming of the lower atmosphere ceases during the day but continues at night. The daytime changes are similar to those found to take place following the emergence of leaves (Schwartz and Karl 1990; Schwartz 1996). Thus, it appears that the springtime reduction in the DTR is linked to the increase in evapotranspiration from emerging vegetation.

Climatologies of the weekly Normalized Difference Vegetation Index (NDVI; not shown) are in qualitative agreement with those of the DTR in the eastern United States during spring in that the DTR maximum usually occurs one to two weeks after the onset of a rapid increase in the NDVI. It is unclear why the DTR maximum does not occur shortly before or exactly at the time of green-up. One possible explanation is a discrepancy between satellite-based measurements of the spring green wave and surface phenology. Schwartz and Reed (1999) found that over the eastern United States, satellite-based estimates of the start of the spring season consistently fell one to two weeks before first leaf emergence dates computed by a "Spring Index Model" from surface meteorological observations. Perhaps the evapotranspiration from the first green leaves sensed by the satellite is not yet sufficient to suppress daytime temperatures in the presence of rapidly increasing clear-day solar radiation. However, a detailed comparison of the DTR and NDVI climatologies is not possible because the determination of the exact time of green-up from the NDVI is complicated by the various uncertainties in the NDVI data, the biweekly resolution

of the NDVI, and a dependence of the NDVI on vegetation type, soil type, and illumination (Reed et al. 1994).

Throughout the summer, the abundant precipitation in this region combined with high temperatures continues to favor high evapotranspiration rates and relatively low values of T_r(pm) and the DTR. Thus, evapotranspiration from soil and vegetation may be responsible not only for the change in slope of the DTR climatology in spring, but also for the subsequent warm season dip in the DTR. The changes in the slopes of T_{max}, T_{min}, T_r(pm), and T_r(am) around the time of the autumn DTR peak represent a reversal of the changes observed in spring. A temporary enhancement of daytime surface heating as a result of the gradual senescence of vegetation may, in part, explain the observed autumn change in afternoon T_r and DTR. However, in agreement with Schwartz's (1990) report of a weaker association during autumn between meteorological conditions and phenological events in honeysuckle and lilac, the change in slope in afternoon T_r is less pronounced in autumn than in spring. A likely reason for the weaker autumn relationship is that the photosynthetic activity of tallgrasses, shrubs, and trees peaks in late spring or early summer and is affected by the amount of moisture available throughout the warm season (Reed et al. 1994), so that the decrease in greenness at the time of senescence is more gradual than the rate of increase during green-up. After the disappearance of green vegetation, the rapidly declining insolation causes the DTR to decline towards its winter minimum.

4.4 Summary

In conclusion, the warm season dip in the DTR appears to be a result of high evapotranspiration rates from vegetation during the day which increase rapidly at the onset of the growing season in spring and continue to be high throughout much of the summer. Before the spring maximum and after the autumn maximum in the DTR, seasonal DTR variations appear to

be controlled largely by seasonal changes in insolation and cloudiness. These findings support Mearns et al.'s (1995) suggestion that the correct simulation of seasonal variations in the DTR, especially during the warm half of the year, requires a detailed and realistic parameterization of soil-vegetation-atmosphere interactions.

Further improvements in the quality of the NDVI and an expansion of ground-based observations of land surface conditions would greatly aid the ability to determine climatological relationships between changes in vegetation and atmospheric conditions. New and expanded surface phenological observing networks which also report measurements of surface evapotranspiration and meteorological variables would be particularly useful in such research efforts.

TABLE 4.1 Average dates of spring and autumn maxima in the diurnal temperature range. Dates are averaged over stations between 80°W and 90°W within 2.5° latitude bands centered on the latitude (Lat, °N) listed on the left. Dates are given in Julian days (Day) and as month/day (MM/DD). The differences (Diff) between the spring and autumn dates are given in days.

Lat	*Spring*		*Autumn*		*Diff*
	Day	*MM/DD*	*Day*	*MM/DD*	*Days*
42.5	144	05/24	268	09/25	124
40.0	133	05/13	272	09/29	139
37.5	117	04/27	285	10/12	168
35.0	107	04/17	294	10/21	187
32.5	107	04/17	310	11/06	203

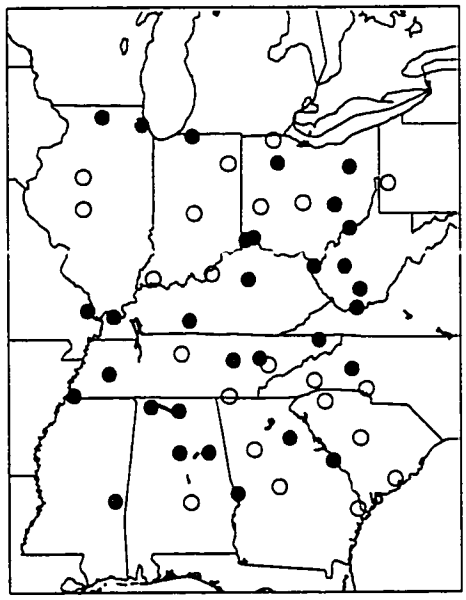

FIGURE 4.1 Map of stations used in this chapter. Open circles indicate locations of stations with sunshine data. Closed circles mark all other stations.

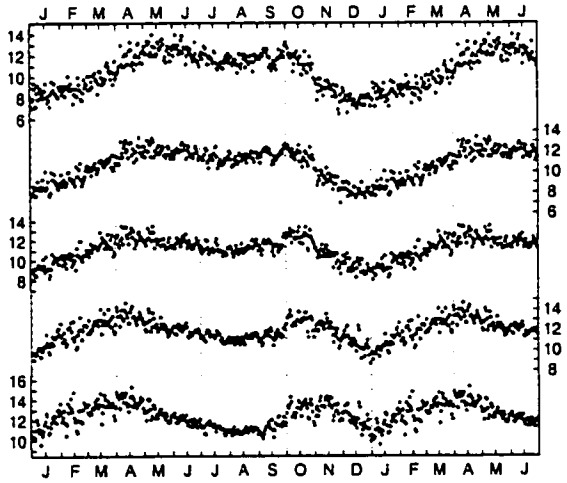

FIGURE 4.2 Climatologies of the diurnal temperature range (DTR, °C) over the eastern United States (80 - 90°W). From top to bottom, the curves represent averages over stations within 2.5° latitude bands centered at 42.5, 40, 37.5, 35, and 32.5°N. Each curve represents one-and-a-half annual cycles. Each dot represents the 1966-1995 average of the DTR for one day of the year.

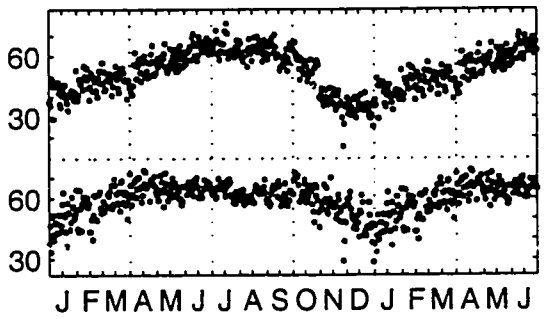

FIGURE 4.3 Climatologies of percent of possible sunshine. The top and bottom curves represent averages over stations within the areas 38.75 - 41.25°N, 80 - 90°W and 31.75 - 33.25°N, 80 - 90°W, respectively. Other plotting conventions are the same as in Figure 4.2.

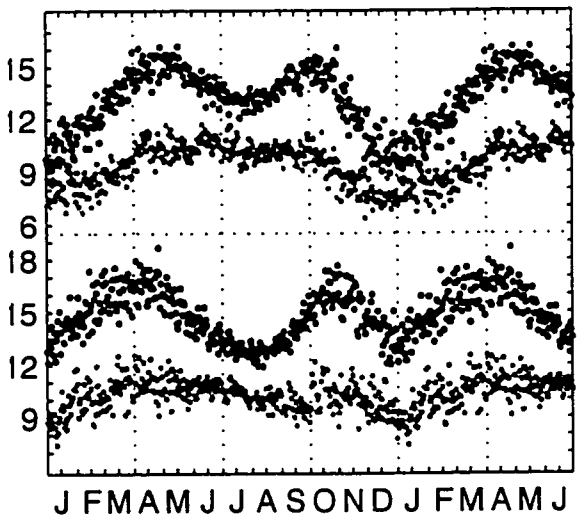

FIGURE 4.4 Climatologies of the diurnal temperature range (°C) on mostly sunny days (black) and other days (gray). The top two curves represent averages over stations within the area 38.75 - 41.25°N, 80 - 90°W. The bottom two curves represent averages over the area 31.75 - 33.25 °N, 80 - 90°W. Other plotting conventions are the same as in Figure 4.2. See text for further explanation.

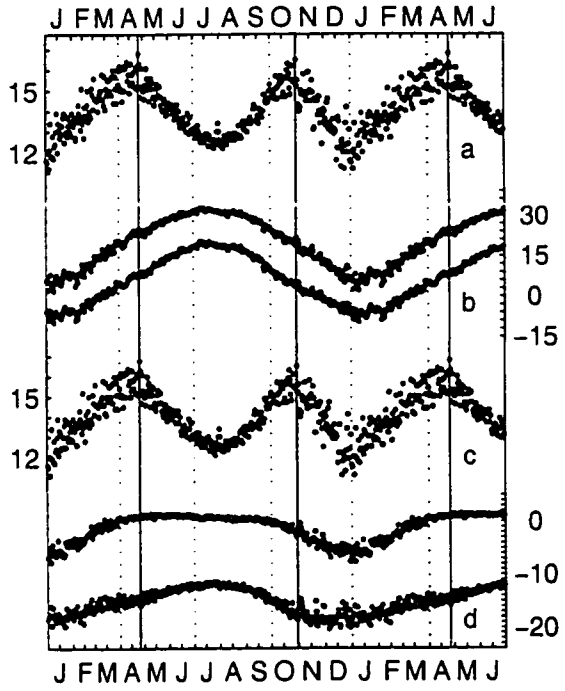

FIGURE 4.5 Climatologies for mostly sunny days. (a) Diurnal temperature range, (b) daily maximum and minimum surface air temperature, (c) the diurnal range of relative surface air temperature, and (d) afternoon and morning relative surface air temperature. Each curve represents 1.5 annual cycles and an average over 22 stations within the study area. Solid vertical lines indicate dates of DTR maxima. All temperatures are in °C.

CHAPTER 5

Factors Influencing the Cold Season Diurnal Temperature Range

5.1 Background

The diurnal temperature range (DTR) has decreased over much of the globe during the past few decades (Karl et al. 1993b; Horton 1995; Easterling et al. 1997). However, some regions, such as the British Isles, the Iberian Peninsula, India, central Canada, and certain coastal areas of North America, have experienced increases in the DTR. Many of these trends have been accompanied by trends in cloud cover that are physically consistent with the DTR changes (Karl et al. 1987; Plantico et al. 1990; Karl et al. 1993b; Dai et al. 1997, 1999), i.e. cloud cover has increased in areas of decreasing DTR and vice versa. Particularly during the cold season, the atmospheric circulation has a strong influence on the distribution of clouds. In addition, the magnitude of day-to-day temperature variability, which has been shown to be positively correlated with the DTR (Karl et al. 1993b), varies in time and space with the frequency of frontal passages and the position of the jetstream. Therefore, the atmospheric circulation should play a significant role in variations of the cold season DTR. However, relatively few studies have considered the possible contribution of changes in the atmospheric circulation to the DTR trends.

Razuvaev et al. (1995) suggested that a decrease in November-March DTR over northern and central parts of the former Soviet Union between 1961 and 1990 may have been caused by an increase in the frequency of synoptic situations that favor warm advection and cyclogenesis. In agreement with this argument, Horton (1995) showed that the Siberian anticyclone was weaker during 1981-1990 than during 1951-1980, and Easterling et al. (1997) demonstrated that an index of surface westerlies based on the Cold Ocean/Warm Land pattern of Wallace et al. (1996) is negatively correlated with the DTR over a region stretching from northern Europe into Russia.

Over the Iberian Peninsula, where precipitation tends to be suppressed when the westerlies over northern Europe are strong (Hurrell 1995; Thompson and Wallace 2000), Easterling et al. found positive correlations between the westerly index and the DTR.

In a recent study, Przybylak (2000) computed mean seasonal DTR over the Arctic for six different synoptic patterns and correlated mean wintertime Arctic DTR anomalies with the North Atlantic Oscillation (NAO) index and the Zonal Index. His results indicate that an increase in cyclonic activity over the Arctic that is associated with a more positive NAO index and stronger zonal flow over mid-latitudes is partially responsible for the observed decrease in Arctic DTR during the winters of 1951-1990.

By the same token, changes in the atmospheric circulation may have contributed to the trends in wintertime DTR over the United States. Based on a comparison of gridded DTR and sea level pressure anomalies for the 1981-1990 period, Horton (1995) suggested that enhanced flow of continental or polar air may have accounted for at least part of the increase in the DTR over the Great Lakes region and the West Coast of the United States between the winters of 1951-1980 and 1981-1990. Such circulation changes may explain the fact that the Pacific Northwest has experienced an increase in DTR and a decrease in cloudiness, whereas most of the contiguous United States has experienced a decrease in DTR and an increase in cloudiness (Plantico et al. 1990; Karl et al. 1993b; Lettenmaier et al. 1994; Elliott and Angell 1997).

Studies of the relationship between total cloud cover over the United States and ENSO variability show that the warm phase of ENSO is associated with below-normal cloudiness over the Northwest and a tendency for above-normal cloudiness over the remainder of the country (Angell and Korshover 1987; Angell 1990; Kane and Gobbi 1995). Other researchers demonstrated that precipitation was suppressed over the Pacific Northwest and enhanced over the southern United States during the positive polarities of the Pacific/North America pattern and

Pacific Decadal Oscillation which prevailed between the late 1970s and mid-1990s (e.g. Leathers et al. 1991; Mantua et al. 1997; Higgins et al. 2000). Croke et al. (1999), on the other hand, found cloudiness over selected regions to be better correlated with variations in the strengths of the climatological-mean surface anticyclones and cyclones than with large-scale circulation patterns. For example, cloud cover in the Northeast is negatively correlated with the strength of the Icelandic low, but poorly correlated with the North Atlantic Oscillation due to a lack of an association with the Bermuda High. Croke et al.'s findings suggest that pre-defined teleconnection patterns may not always capture the full extent to which regional variations of a certain meteorological variable are related to the atmospheric circulation.

A few studies have investigated the possibility that changes in snow cover extent over North America have contributed to the observed DTR trends (Cerveny and Balling 1992; Karl et al. 1993b), but collectively, their findings have been inconclusive. The hypothesis of an association between trends in snow cover extent and the DTR is based on the fact that, due to the high albedo of snow, daytime temperatures and the DTR tend to be lower over snow than over bare ground (Dewey 1977; Ruschy et al. 1991; Karl et al. 1993a,b; Leathers et al. 1995; Groisman et al. 1996; Hughes and Robinson 1996; Kalkstein et al. 1996). Recent work by Groisman et al. (2000) and Sun et al. (2000) indicates that snow cover affects not only temperature itself, but also the relationship between cloudiness and temperature. Because the cloud albedo is generally closer in magnitude to the albedo of snow than to the albedo of bare ground, the influence of clouds upon daytime surface air temperature is reduced when the ground is blanketed with snow. Based on these findings, it appears that the combined effects of cloudiness and snow cover play an important role in variations of the DTR.

The main goal of this chapter is to determine to what extent long-term changes in cloudiness, snow cover, and atmospheric flow patterns account for both the widespread downtrends in the

DTR and regional differences in DTR trends across the contiguous United States. A number of correlation, regression, and linear trend analyses are performed on daily surface and lower-tropospheric data, focusing on the cold season months (November through March) when the influence of teleconnection patterns on surface climate tends to be strongest.

Employing simple linear regression, patterns of 1000-mb geopotential height (a surrogate for sea level pressure) are derived that explain the maximum possible fraction of the daily variance in the DTR. The configuration of these patterns for different regions as well as correlations between the associated index time series and various meteorological variables provide information on the mechanisms by which the geopotential height field influences the regional DTR. The correlation analysis includes not only surface variables such as daily maximum and minimum temperatures, sunshine duration, and snow cover extent, but also the difference in temperature between the surface and 850-mb level which serves as a crude measure of the static stability of the atmospheric planetary boundary layer. The index time series are also used to assess the contribution of the DTR-related height patterns to trends in regional cold-season DTR between 1965/66 and 1994/95. The distinction between this methodology and a correlation or regression analysis that involves indices of well-known circulation patterns, such as the Arctic Oscillation, is that the configurations and spatial scales of circulation patterns are not determined a priori.

The chapter is organized as follows. Section 5.2 describes the data and some basic analysis techniques used. The relationships between the DTR, cloudiness, and snow cover in eight regions of the United States are documented in Section 5.3. In Section 5.4, the DTR-associated circulation pattern for each of the eight regions is derived, and its impact on the DTR is discussed. Trends in the DTR and the contributions of changes in cloudiness, the atmospheric circulation, and snow cover extent to these trends are described in Section 5.5. The chapter concludes with a summary and discussion of the results in Section 5.6.

5.2 Data and Analysis Techniques

Daily maximum and minimum temperatures (T_{max} and T_{min}), percent of possible sunshine (p_{sun}), and snow depth are extracted from the First Order Summary of the Day (FSOD) dataset (France 2000). Daily-mean and monthly-mean 1000-mb heights as well as 00Z and 12Z 850-mb temperatures from the NCEP/NCAR Reanalysis (Kalnay et al. 1996) are also used. In addition, homogeneity-adjusted monthly-mean maximum and minimum temperatures at 1041 mostly rural United States stations in the Global Historical Climatology Network (GHCN; Peterson and Vose 1997) are utilized in some of the trend analyses of Section 5.5. All of these datasets are described in more detail in Chapter 2. The period of study is 1958-1995, which includes 37 cold seasons (November-March 1958/59 through 1994/95).

The FSOD stations chosen for the analyses of this chapter are shown in Figure 5.1. It is clear from the map of station locations that far fewer high-quality stations are located in the western half of the country than in the eastern half. The stations have been grouped into eight regions based on geographical homogeneity (Fig. 5.1). No region is defined for the interior mountain west because of the paucity of stations and the large inter-station variability in this part of the country. High-quality records of snow depth and p_{sun} are available for only a subset of the chosen stations, and observations of p_{sun} do not begin until 1965 in the FSOD dataset.

The difference in temperature between the surface and 850-mb level (TD) is used as a relative measure of boundary layer stability. For the morning hours, TD at a particular station is estimated by subtracting the 12Z 850-mb temperature at the nearest grid point from the local daily minimum temperature. For the afternoon, the day's local maximum temperature and the next day's 00Z 850-mb temperature are used to calculate TD. The morning and afternoon surface-to-850-mb temperature differences are denoted by TD_{am} and TD_{pm}, respectively, and are computed only for stations at elevations below 700 m.

For each variable and each station or grid point, time series of daily values are formed for the November-March season. Next, the seasonal cycle is removed from all time series by subtracting from each daily value the day's climatological mean, defined as the 37-year mean for that date. When standardized values are required, the daily anomalies are divided by the standard deviation of all values in the time series.

Simple linear correlations and trends based on least-squares regression are used extensively throughout this chapter. The statistical significance of the correlations is tested with the t-statistic, for which the number of independent samples is found by applying Leith's (1973) formula to both time series and choosing the smaller of the two resulting values. A correlation is considered to be meaningful if it is statistically significant at the 5% level. To test the statistical significance of the linear trend in a particular time series, the t-statistic is applied to the correlation between the time series and time (i.e. the sequence of dates associated with the time series), using the number of independent samples in the time series.

A frequently cited disadvantage of least-squares regression is its sensitivity to outliers and endpoints. In addition, the underlying assumption that the variables to which the method is applied are normally distributed is frequently violated by daily values of meteorological variables in general and the diurnal temperature range and percent of possible sunshine in particular (Karl et al. 1993b; Lanzante 1996). In order to test for the importance of these factors in the results presented here, some of the analyses have been repeated using Pearson rank-order correlations as well as trends based on median of pairwise slopes regression (Lanzante 1996). These non-parametric techniques are resistant to outliers, do not emphasize the endpoints of time series, and do not require the variables to be normally distributed. To calculate the Pearson rank-order correlation between two time series x and y, the values of each time series are first ranked, and then the correlation coefficient between the resulting time series of ranks is computed. In median

of pairwise slopes regression, the slope of the regression line is defined as the median of slopes between all possible pairs of points within the time series. Since this method necessitates the computation of (N-1)! slopes for a time series of length N, it was applied to time series of monthly averages rather than daily values. The correlations and trends obtained with the non-parametric methods turn out to be nearly identical in sign and similar in magnitude to those based on parametric techniques. Therefore, only the results based on the more widely used parametric techniques are shown.

In order to address concerns regarding possible effects of urbanization and changes in instrumentation and station location on temperature and DTR trends based on the FSOD data, the GHCN temperature data are used for a comparison of DTR trends computed from the two datasets. In general, the validity and importance of the trend in a particular variable are judged based on statistical significance, physical consistency with trends in other variables, and consistency with previously reported trends.

5.3 Regional DTR-Cloudiness Relationships and the Influence of Snow Cover

Table 5.1 displays the November-March correlation coefficients between daily anomalies of p_{sun} and the DTR for each of the regions outlined in Figure 5.1. These correlations are derived by first computing the daily anomalies of the DTR and p_{sun} at each station and then correlating the anomalies for all station-days within a region. The limited availability of sunshine duration observations restricts this analysis, and all other analyses presented in this section, to the period 1965/66-1994/95 and to a subset of stations, as indicated in Figure 5.1. The DTR-p_{sun} correlations, which are all statistically significant at the 99.9% level, demonstrate the strong relationship between cloudiness and the DTR. However, they also show that the DTR-p_{sun} association is not as strong in the north-central and northeastern states as in other parts of the

country. Dai et al. (1999) found cold-season correlations between the DTR and total cloud cover to be weaker at middle and high latitudes in the Northern Hemisphere than at lower latitudes and attributed this result to the decrease in insolation with increasing latitude. This argument is supported by Sun et al.'s (2000) finding that the daytime cooling effect of clouds increases as the solar elevation angle increases. Thus, the north-to-south gradient in the correlations between the DTR and p_{sun} to the east of the Rocky Mountains is consistent with a southward increase in insolation. In the western United States, however, the relationship between p_{sun} and the DTR is as strong at the coastal stations in the Pacific Northwest as in the Southwest, despite the meridional gradient in insolation.

The relatively weak correlations between the DTR and p_{sun} in the north-central and northeastern United States could also be an indication of the effects of snow cover since the influence of clouds on daytime surface air temperatures is reduced by the presence of snow on the ground (Groisman et al. 1994, 2000; Sun et al. 2000). Figure 5.2 shows seasonal variations of the DTR between November 1st and March 31st in the northern Great Plains for clear (black) and cloudy (gray) days on which either no snow is on the ground (top) or the snow depth equals at least 2.5 cm (bottom). A day is considered to be clear if p_{sun} exceeds 90%, while days with $p_{sun} <$ 10% fall into the cloudy category. The figure is constructed using observations at seven stations for the cold seasons of 1965/66 to 1994/95. Each dot in the figure represents a seven-station DTR average for one of the four categories of days on a particular calendar date.

It is evident from the top panel of Figure 5.2 that on snow-free days throughout the cold season, the clear-sky DTR is higher than the cloudy-sky DTR. This relationship between the DTR and cloudiness is consistent with the results of Karl et al. (1987), Plantico et al. (1990), Karl et al. (1993b), and Groisman et al. (1996). In agreement with the findings of Groisman et al. (1994, 2000) and Sun et al. (2000), the difference in DTR between clear and cloudy days is less

pronounced for days with snow on the ground, primarily because the clear-sky DTR is smaller. The DTR is least sensitive to both snow cover and cloudiness in mid-winter when clear-sky solar radiation is at its minimum, as expected from analyses by Leathers et al. (1995) and Groisman et al. (1996).

In order to assess the extent to which snow cover influences the relationship between the DTR and p_{sun} in different regions of the United States, correlations between the DTR and p_{sun} have been computed separately for station-days with no snow on the ground (no SOG) and for station-days with a snow depth of at least 2.5 cm (SOG). These correlations, as well as the percentage of days in each of the two categories, are shown in Table 5.1. In addition, regional-average DTR anomalies have been calculated for the same four categories of days used to construct Figure 5.2: clear no-SOG days, clear SOG days, cloudy no-SOG days, and cloudy SOG days (Table 5.2). Due to the rare occurrence of snow in the southern states and coastal Northwest, SOG-day correlations and average DTR anomalies are not presented for those regions. The stations included in these analyses are indicated by the concentric circles in Figure 5.1, and the number of stations in each region is listed in Table 5.1. The number of station-days in each of the four categories used to construct Table 5.2 exceeds 2000 in all but two cases and ranges from 811 in the clear SOG group for the southern Plains to 18468 in the cloudy no-SOG category for the Midwest.

In every region in which both SOG and no-SOG categories are represented, the correlation between the DTR and p_{sun} is higher without snow on the ground than in the presence of snow, although the association between the two variables is highly statistically significant for both categories of days (Table 5.1). The clear-sky DTR is consistently higher in the no-SOG category than in the SOG category, whereas the presence of snow appears to have little impact on cloudy-

sky DTR (Table 5.2). These findings are consistent with a lowering of daytime temperatures due to the high albedo of snow (Groisman et al. 1996, 2000; Sun et al. 2000).

The depression of the overall correlation relative to the no-snow correlation is largest in the northern Plains where fewer than half of the days are snow-free, and the difference between the no-SOG and SOG correlations is largest. The Great Plains have previously been identified as the region of the United States in which the relationship between maximum temperature and snow cover extent is strongest (Dewey 1977; Karl et al. 1993a). The correlation on SOG days in the northern Plains might be higher if it were not for the increase in the DTR between cloudy snow-free days and cloudy SOG days. The relationship between the DTR and snow cover on cloudy days may be a result of a more rapid drop of nighttime temperatures over a snow-covered surface than over bare ground (Dewey 1977; Karl et al. 1993b; Leathers et al. 1995). Nevertheless, the snow-related increase in the DTR on cloudy days does not offset the decrease on clear days. Both the correlations and average DTR anomalies indicate that in the southern Plains, the association between the DTR and p_{sun} remains relatively strong when snow is present, even though one might expect the more intense insolation in this region to enhance the albedo effect (Karl et al. 1993b). Compared to the northern Plains, more rapid melting between snowstorms in the southern Plains is likely to decrease the snow albedo and, therefore, the impact of snow on daytime temperatures (Robock 1980; Leathers et al. 1995).

In the Northeast, the relationship between the DTR and cloudiness is relatively weak, regardless of whether snow is present. The difference between clear-sky and cloudy-sky DTR is barely larger without snow on the ground than in the presence of snow. Wagner (1973) and Leathers et al. (1995) found that the sensitivity of temperature to snow decreases towards the Atlantic coast, suggesting that the moderating influence of the ocean weakens the snow cover-temperature relationship. In addition, Robock (1980) noted that forested areas experience a much

smaller snow-related change in surface albedo and daytime temperature than open, flat surfaces. Thus, both coastal influences and surface type may be responsible for the nearly negligible impact of snow cover on the DTR in the Northeast.

In summary, the presence of snow cover leads to a smaller clear-sky DTR in much of the central and northeastern United States. The relationship between the DTR and p_{sun} is most strongly affected by snow in the northern Plains. The strength of the associations between the DTR, cloudiness, and snow cover varies geographically depending on insolation, the frequency of snow cover and cloudiness, proximity to the ocean, and vegetation type. These findings will be taken into consideration where appropriate in the following sections.

5.4 DTR-Related Circulation Patterns

5.4.1 Procedure

In this section, 1000-mb geopotential height patterns associated with daily variations in regional DTR are examined and interpreted in the context of contemporaneous variations in other meteorological variables. Each pattern is derived by regressing time series of daily geopotential height anomalies at each grid point within the North American sector (20°N - 60°N, 40°W - 140°W) onto a time series of daily standardized regional-mean DTR. This procedure yields eight regional regression patterns – one for each of the regions of the United States outlined in Figure 5.1. Index time series that provide a measure of the temporal variations of the derived patterns are then formed by regressing daily maps of standardized geopotential heights onto a standardized version of each pattern. For the derivation of the circulation index time series of a particular region, only the portions of the 1000-mb height maps and regression pattern which fall within the area of the region of interest are used. The configuration of the patterns as well as the correlation of the index time series with the DTR, p_{sun}, and other meteorological variables are used to assess

the statistical and physical significance of the patterns.

For this analysis, the 37 cold seasons (November-March) between 1958/59 and 1994/95, which comprise a total of 5596 days, are used. Regional DTR averages are computed for each of the eight regions (Fig. 5.1) by arithmetically averaging values from all stations within the region. A regional average for a particular day is formed only if a DTR value is available at more than 70% of the stations within the region. Otherwise, the day's regional average is considered as missing and is not included in any subsequent calculations. The regional-mean DTR time series are standardized by first subtracting the calendar day's climatological mean from each data point and then dividing by the overall standard deviation of the regional time series. Analogous regional averages and anomalies are computed for T_{max}, T_{min}, p_{sun}, TD_{pm}, and TD_{am}. For each variable, all stations with a high-quality record of that variable are used (Fig. 5.1). In the case of TD_{pm} and TD_{am}, only stations at elevations below 700 m are included.

The dimensions of the domain used for the derivation of the circulation index time series associated with each regression pattern was chosen based on the configuration of the pattern and experiments with domains of different sizes. When computing the index time series for a particular region, using only the 1000-mb heights and regression coefficients within the region of interest yielded more consistent results than using a larger domain.

Figure 5.3 displays the 1000-mb height regression patterns for all eight regions. The regression coefficient at each grid point represents the change in geopotential height (in meters) associated with a one-standard deviation positive anomaly in regional DTR. Since, by definition, the patterns are linearly related to the regional DTR, a one-standard deviation negative DTR anomaly is associated with 1000-mb height anomalies that are equal in magnitude, but opposite in sign to those shown in Figure 5.3.

Table 5.3 gives correlations between the daily index time series associated with each pattern

and anomalies of regional-average DTR, p_{sun}, T_{max}, T_{min}, TD_{pm}, and TD_{am}. Since the presence of snow cover can reduce the effect of variations in cloudiness on the DTR, it may also impact the relationship between the derived circulation patterns and the surface climate. For this reason, the correlations of the pattern indices with the DTR and p_{sun} on snow-free days are also calculated for the northern and southern Plains, Midwest, and Northeast. A day is defined as snow-free in a particular region if none of the stations with adequate snow depth data within the region report snow on the ground.

Among the correlations in Table 5.3, only those with magnitudes less than 0.08 are not significant at the 5% level. Thus, based on the correlations between the DTR and the circulation indices, all eight regional circulation patterns are highly statistically significant. The significance of the patterns is further corroborated by the fact that very similar and physically consistent results are obtained when the same procedure is applied to 500-mb heights alone or to a combination of 500-mb and 1000-mb heights (not shown).

5.4.2 Description of the Circulation Patterns

The regression patterns for the Northeast, Midwest, and Southeast are shown in Figures 5.3a-c. In all three cases, the DTR is high when much of the region is located in the northern or northwestern portion of an anomalous surface anticyclone. The configuration of these patterns suggests that the depicted synoptic situation represents a transition from anticyclonic control to cyclonic control. This impression is confirmed by one-day lead and lag regression patterns (not shown) which show a progression of the high pressure center from west to east across the region of interest. The patterns further imply that the affected region is dominated by an anomalous southwesterly to westerly low-level flow of relatively dry continental air over the area. Conversely, below-normal DTR is observed when easterly wind anomalies and relatively moist marine air prevail.

As can be seen from Table 5.3, the circulation index time series for the three regions are positively correlated with TD_{pm}, T_{max}, and T_{min}, negatively correlated with TD_{am}, and not well-correlated with p_{sun}. These correlations imply a tendency for the afternoon boundary layer to be more unstable and the nighttime boundary layer to be more stable on days with above-normal DTR than on days with below-normal DTR. They further indicate that the positive polarity of the DTR-related circulation pattern tends to be associated with warmer surface air temperatures than the negative polarity.

Panels d-f of Figure 5.3 show the DTR-related patterns for the northern Plains, southern Plains, and south-central states. In each case, the DTR tends to be high when positive 1000-mb height anomalies centered to the south of the region and a broad area of below-normal heights centered to the north act to produce anomalous westerly geostrophic flow over the region. These patterns are reminiscent of synoptic situations in which the region of interest is under the influence of a lee trough. The correlations between the circulation index time series and the DTR are larger than over the eastern United States and increase from 0.45 in the northern Plains to 0.56 in the south-central states. The correlation between p_{sun} and the corresponding circulation index varies from 0.16 in the north to 0.43 in the south. When only days without snow on the ground are considered, the northern Plains correlations are raised to levels comparable to those found in the southern Plains, that is 0.56 for the DTR and 0.27 for p_{sun}. As in the eastern United States, the circulation indices for the central states are positively correlated with TD_{pm}, T_{max}, and T_{min} as well as negatively correlated with TD_{am}.

These correlations suggest that the circulation patterns derived for the central United States affect the DTR to some extent by varying the strength of solar heating of the surface during the day. Schwartz and Skeeter (1994) found that continental air, which generally favors clear skies, dominates the north-central United States when a surface high is located over the center of the

country. The conditions depicted in Table 5.3 and panels d-f of Figure 5.3 may also be linked to adiabatic warming of Pacific air during its descent on the lee side of the Rocky Mountains (Kalkstein et al. 1996). When a central United States pattern is in its negative polarity, below-normal heights are found to the south of the DTR region, and upslope flow on the eastern side of the Rocky Mountains results in relatively cool, cloudy, low-DTR weather over the affected region in the central United States.

In the Southwest, a high DTR is associated with above-normal 1000-mb heights centered near the northern edge of the region (Fig. 5.3g). The configuration of the geopotential height field in Figure 5.3g somewhat resembles synoptic-scale patterns that have been linked to subsidence and an absence of storms in the Southwest (Davis and Walker 1992; McCabe and Legates 1995). The time series of the Southwest circulation pattern is strongly negatively correlated with TD_{am} (-0.42), weakly negatively correlated with T_{min}, and weakly positively correlated with p_{sun} (0.23) and T_{max} (0.20). The correlations imply that the positive polarity of the DTR-related pattern primarily favors an unusually stable boundary layer at night, while the negative polarity favors less stable nighttime conditions.

The 1000-mb height pattern linked to above-normal DTR along the Pacific coast of the northwestern United States features strong positive anomalies centered approximately over Vancouver Island (Fig. 5.3h). This situation is favorable for fair weather over the Northwest as well as a Pacific storm track that is displaced northward or southward from its climatological-mean position (Skeeter and Park 1985; Leathers et al. 1991; Davis and Walker 1992; McCabe and Legates 1995). Daily variations in this circulation pattern are strongly positively correlated with the DTR (0.55) and p_{sun} (0.54) and are negatively correlated with T_{min} (-0.54) and TD_{am} (-0.50). Thus, compared to the negative polarity, the positive polarity of this region's DTR-related circulation pattern is linked primarily to sunnier days and colder, more stable nights.

In summary, the DTR-related circulation patterns explain between 11% and 30% of the daily variance of the DTR in all regions. Figure 5.3 and Table 5.3 indicate that high (low) diurnal temperature ranges tend to occur in situations in which a high (low) pressure system is centered over or near the area such that dry or continental (moist or marine) air is flowing over the region. Specifically, a high DTR is favored by westerly surface winds in areas to the east of the Rockies and easterly winds in regions of the western United States.

The correlations between the circulation pattern indices and nighttime surface-to-850-mb temperature differences are negative across the entire country. To the east of the Rockies, the positive polarities of the patterns are associated with an anomalously unstable afternoon boundary layer as well as above-normal T_{max} and T_{min}. The relationship between the circulation indices and p_{sun} is strong only in the south-central states and coastal Northwest, suggesting that other, unidentified processes also contribute to the correlations between the index time series and the DTR. Considering the consistently negative index-TD_{am} correlations, these processes may include those affecting the stability of the nighttime boundary layer.

None of the circulation pattern indices is well-correlated with snow cover extent (not shown). However, in the northern Great Plains, the index-DTR and index-p_{sun} correlations improve when only snow-free days are considered (Table 5.3), since the presence of snow tends to weaken the relationship between the DTR and cloudiness (Tables 5.1 and 5.2).

When the analyses of this section are performed on monthly-mean data, the resulting DTR-related circulation patterns (not shown) are qualitatively similar to those obtained from daily data. This finding suggests that the relationships between the circulation patterns and surface meteorological conditions described here are present not only at daily time scales, but also at monthly and longer time scales.

5.5 Observed Cold Season DTR Trends and Contributing Factors

In light of the results of the previous two sections, it appears that changes in cloudiness, snow cover, and the atmospheric circulation could all conceivably be contributing to long-term trends in the cold season DTR. Karl et al. (1987), Plantico et al. (1990), Karl et al. (1993b), and Dai et al. (1997, 1999) have argued that much of the widespread decrease in the DTR since the 1950s can be attributed to an increase in cloudiness. However, as shown in Section 5.3, changes in the frequency or extent of snow cover may, in certain regions, have a significant influence on clear-sky DTR and may therefore also affect the overall DTR trends. In addition, an analysis of trends in the circulation pattern indices derived in the previous section should permit at least a preliminary assessment of the contribution of changes in the atmospheric circulation to the observed DTR trends.

5.5.1 Observed Cold Season Trends for 1965/66-1994/95

Maps of observed linear trends in the DTR, percent of possible sunshine, and 1000-mb height for the 30 cold seasons between 1965/66 and 1994/95 are shown in Figures 5.4 and 5.5. In addition, the 1965/66-1994/95 cold season trends of various variables have been calculated from time series for the eight regions outlined in Figure 5.1 (Table 5.4). Regional averages of the DTR, T_{max}, T_{min}, p_{sun}, TD_{am}, and TD_{pm} are formed as described in Section 5.4.1. A proxy for snow cover extent within a particular region is created by computing, for each day of the record, the percentage of stations within the region that report a snow depth of at least 2.5 cm. For this calculation, only stations with high-quality records of snow depth, T_{max}, T_{min}, and p_{sun} are used. These stations are identified by concentric circles in Figure 5.1. A regional daily percentage is computed when snow depth data are available at all of the eligible stations within a region; otherwise, the day's regional value is flagged as missing. The resulting regional time series is an

approximate measure of the snow cover extent within the region. As such, it is easily compared to daily time series of regional averages of other variables.

As described in Section 5.2, the statistical significance of all trends is determined by applying a Student's t-test to the correlations between the time axis and time series. Trends significant at the 10% level are indicated by closed circles in Figure 5.4. Trends significant at the 5% level are marked by concentric circles in Figure 5.4 and are printed in boldface type in Table 5.4. In Figure 5.5, the magnitudes of trends are indicated by geopotential height contours in order to facilitate a comparison of the pattern of 1000-mb height trends with the DTR-related circulation patterns shown in Figure 5.3.

On a national scale, negative (gray) DTR trends dominate over positive (black) DTR trends in Figure 5.4a. Decreases in the DTR are found over the central and southern United States, although the regional-mean trends in the Great Plains and Southeast are not significant at the 5% level (Table 5.4). The Northeast, portions of the Northwest and northern Rockies, as well as some locations along the Gulf Coast have experienced an increase in the DTR, while the trends are of mixed sign in the Midwest. The DTR trends are accompanied by a considerable warming, with a larger rise in T_{min} than in T_{max} (Table 5.4). In fact, T_{min} has risen in all regions except the coastal Northwest, while T_{max} has increased everywhere except over the south-central states.

Many previous analyses of DTR trends over the United States were based on periods of record beginning in the 1940s or early 1950s and ending in the 1980s or early 1990s (Karl et al. 1984, 1987; Plantico et al. 1990; Karl et al. 1993b; Lettenmaier et al. 1994; Knappenberger et al. 1996). Because linear trends are highly sensitive to the period of record chosen, a detailed comparison of Figure 5.4a with the results of these earlier studies is difficult. In addition, differences in datasets and analysis techniques may contribute to disparaties among the results. It is remarkable, however, that a preponderance of negative DTR trends over the United States as a

whole and the southern states in particular as well as the warming over the western states and northern Plains are common to all of these studies. The cooling over the eastern United States that is noted in many of the earlier studies is present neither in the results of this study nor in the results of Gaffen and Ross (1999) and Higgins et al. (2000) whose periods of record extend from the early 1960s through the early 1990s. A comparison of the cold season temperature trends for 1950-1995 and 1966-1995 in the GHCN dataset indicates that the cooling trends are particular to the longer 1950-1995 period, while a warming prevails over the eastern United States when the period of record is limited to 1966-1995. Thus, the differences among previously published trends for this region can be attributed to the different periods of record used.

Compared to the trends in T_{max} and T_{min}, the trends in the surface-to-850-mb temperature differences are less spatially coherent in sign and generally smaller in magnitude (Table 5.4). Notable exceptions are found in the two western regions in Table 5.4. While both TD_{pm} and TD_{am} have decreased significantly in the coastal Northwest, they have increased significantly in the Southwest. The fact that, in the Pacific Northwest, the TD_{pm} and TD_{am} trends are negative and larger in magnitude than the T_{max} and T_{min} trends may be interpreted as indicative of a warming at the 850-mb level relative to the surface. Conversely, in the Southwest, the rise in surface air temperatures and surface-to-850-mb temperature differences could be viewed as a reflection of a warming of the surface relative to the 850-mb level that is particularly pronounced at night.

Trends in sunshine duration have been mostly downward over the southern United States and strongly upward over the Pacific Northwest (Fig. 5.4b, Table 5.4). Over the remainder of the country, trends are small and vary in sign. These findings are in qualitative agreement with those of many other studies (Karl et al. 1987; Angell 1990; Plantico et al. 1990; Kane and Gobbi 1995; Elliott and Angell 1997). The spatial pattern of trends in the DTR (Fig. 5.4a) is physically consistent with the pattern of trends in p_{sun} (Fig. 5.4b): areas of increases in the DTR are

approximately collocated with areas of increasing sunshine duration, while areas of decreasing DTR are found where p_{sun} has also been decreasing. Together with the rather strong, positive correlations between the DTR and p_{sun} shown in Table 5.1, the similarity between the patterns of trends in Figures 5.4a and 5.4b supports the conclusion of Karl et al. (1987), Plantico et al. (1990), and Dai et al. (1997, 1999) that changes in cloudiness are likely to have contributed significantly to the observed changes in the DTR. Due to the paucity of stations with continuous long-term records of p_{sun} over vast portions of the western United States, a detailed analysis of this trend relationship is beyond the scope of this study. However, the linear contributions of trends in sunshine duration to regional-average trends in the DTR will be discussed briefly in the next subsection.

The only region with a statistically significant change in snow cover extent is the Northeast where the number of stations reporting a snow depth of at least 2.5 cm has decreased by 11% over the 30-year period examined (Table 5.4). While trends in snow cover extent for the Northeast during this period of record do not appear to be well-documented in the literature, the lack of significant trends in the Midwest and Great Plains is consistent with the work of Leathers et al. (1993), Brown et al. (1995), and Hughes and Robinson (1996). Due to the weak relationship between snow cover and the DTR in the Northeast (Table 5.2) as well as the insignificant trends in snow cover extent in other regions (Table 5.4), the linear contributions of snow cover extent to long-term changes in the DTR are negligible and will not be further analyzed during the course of this study.

The pattern of trends in 1000-mb heights in Figure 5.5 indicates falling heights over the central North Pacific, from 55°N northward over eastern Canada, and from 50°N northward over the North Atlantic. Rising heights are found across the rest of the domain, with maxima over the northern Rockies and subtropical North Atlantic. The 1000-mb height patterns associated with

variations in the DTR over the southern Plains (Fig. 5.3e), south-central states (Fig. 5.3f), Southwest (Fig. 5.3g), and coastal Northwest (Fig. 5.3h) project, at least to some extent, onto the trends shown in Figure 5.5. The tendency towards higher pressure over the Rocky Mountains is consistent with the 1976/77 jump in the Pacific Decadal Oscillation (Mantua et al. 1997), while the changes over the Atlantic are consistent with the trends in the Arctic Oscillation and North Atlantic Oscillation between the 1960s and 1990s (Hurrell 1995; Thompson and Wallace 1998). The contributions of these changes in the 1000-mb height field to trends in the DTR will be discussed in the next subsection.

In summary, the most coherent interrelationships among trends of different variables are found in the coastal Northwest where the increases in the DTR and daily maximum temperature are accompanied by physically consistent increases in sunshine duration, boundary-layer stability, and the DTR-related circulation pattern index. In the south-central and southeastern United States, the trends in both sunshine duration and the DTR-related circulation indices also are of the same sign as the observed trend in the DTR. However, in contrast to the positive trends in the Northwest, the trends of the DTR, p_{sun}, and the regional circulation index are negative. Based on the 1000-mb height trends shown in Figure 5.5 as well as the signs of trends in the DTR and cloudiness reported for various periods of record (Karl et al. 1984; Angell 1990; Plantico et al. 1990; Lettenmaier et al. 1994; Kane and Gobbi 1995; Gaffen and Ross 1999), these changes may be related to the 1976/77 shift in the Pacific Decadal Oscillation. In the Southeast, the Arctic Oscillation may also have played a role in the observed long-term changes (Higgins et al. 2000).

5.5.2 Contributions of Sunshine Duration and Circulation Patterns to Cold Season DTR Trends

Table 5.5 shows the residual DTR trends obtained by removing the linearly congruent contributions of either sunshine duration (C_{sun}) or the DTR-related circulation pattern index (C_{circ}) from the total regional 1965/66-1994/95 cold season DTR trends by means of simple linear

regression. If b_{sun} (in °C $\%^{-1}$) and b_{circ} (in °C (standard deviation)$^{-1}$) are the slopes of the DTR-p_{sun} and DTR-circulation index regression lines, and if T_{DTR}, t_{sun}, and t_{circ} are the cold season trends in the DTR, percent of possible sunshine, and the circulation index, respectively, then the contributions C_{sun} and C_{circ} are computed as follows:

$$C_{sun} = b_{sun} \times t_{sun} \qquad (5.1a)$$

and

$$C_{circ} = b_{circ} \times t_{circ} \qquad (5.1b).$$

The corresponding residual trends R_{sun} and R_{circ} are calculated according to the equations

$$R_{sun} = t_{DTR} - C_{sun} \qquad (5.2a)$$

and

$$R_{circ} = t_{DTR} - C_{circ} \qquad (5.2b).$$

In addition, multiple regression is applied to remove the contributions of both the circulation pattern index and sunshine duration from the total DTR trends. Using the multiple regression coefficients k_{sun} and k_{circ}, the residual DTR trend, R_{both}, is defined as

$$R_{both} = t_{DTR} - k_{sun} \times t_{sun} - k_{circ} \times t_{circ} \qquad (5.3).$$

When compared to the overall DTR trends, the residual trends provide a quantitative estimate of the fraction of the trends that is not "linearly congruent" with the DTR-related circulation patterns or cloudiness.

The residual R_{circ} has also been calculated at each station shown in Figure 5.1. The station-by-station calculation permits the derivation of index time series of DTR-related variations in the 1000-mb height field and corresponding residual trends for all available stations, including those located in data-sparse areas for which no analysis regions have been defined. First, DTR-related 1000-mb height patterns and associated index time series are computed using daily time series of

DTR anomalies at each station in place of regional-average time series. This computation generates a regression pattern analogous to those in Figure 5.3 for each of the 213 stations. For the computation of the circulation index related to the DTR at a particular station, only the portion of the regression and 1000-mb height anomaly maps within a 10° latitude × 10° longitude box centered on the station are used. The dimensions of this area have been chosen based on the sizes of the eight analysis regions used in Section 5.4 and a series of calculations in which the area of the box was varied.

Maps of the contributions of the DTR-related circulation pattern indices to the station DTR trends for box sizes of 5° × 5°, 10° × 10°, and 15° × 15° are shown in Figure 5.6. The contribution at each station is expressed as a percentage of the station's 1965/66-1994/95 cold season DTR average. Although some differences among the three maps are apparent, the overall spatial pattern of the contributions remains qualitatively the same as the size of the box around the station is increased. Therefore, the intermediate box size of 10° × 10° has been chosen.

The residual trends are then determined by applying Equation 5.1b at each station and computing the trends of the resulting residual DTR time series. The total and residual 1965/66-1994/95 trends in cold season DTR, again expressed as percentages of the DTR averages for the same period, are shown in Figure 5.7. An analogous set of residual trends following the removal of variations due to p_{sun} is not shown due to the inadequate spatial coverage of high-quality sunshine records (Fig. 5.1).

The same station-by-station analysis has been performed using monthly-mean maximum and minimum temperatures from 1041 GHCN stations and monthly-mean 1000-mb heights from the NCEP/NCAR Reanalysis. In contrast to the FSOD dataset, the GHCN consists mainly of rural stations whose data records have been adjusted for changes in station location, instrumentation, and observing practices (Peterson and Vose 1997). Therefore, any differences in the spatial

pattern of trends computed from the two datasets can be attributed to differences in the geographical distribution of stations as well as the adjustments applied to the GHCN data. Maps of the total and residual DTR trends at GHCN stations for the cold seasons of 1965/66-1994/95 are shown in Figure 5.8.

The removal of the variability due to p_{sun} from the DTR time series reduces the negative DTR trends over the south-central and southeastern states to near zero (Table 5.5). In addition, the magnitudes of the negative trend in the Southwest and the positive trend in the coastal Northwest are decreased by 25% and 37.5%, respectively, but the trends of the residual DTR time series in those regions remain statistically significant. These findings suggest, in agreement with previous studies by Karl et al. (1987) and Plantico et al. (1990), that increases in cloudiness over the southern United States and decreases over the coastal Northwest contribute to the observed trends in the DTR. In the north-central and northeastern parts of the country, however, relatively low correlations between the DTR and p_{sun} (Table 5.1) and/or negligible trends in p_{sun} (Table 5.4) yield residual DTR trends that nearly equal the total DTR trends. Neither in these regions nor in the southern Plains do the trends in the DTR during the cold season appear to be related to linear trends in sunshine duration.

Judging from Table 5.5 and Figures 5.7 and 5.8, the removal of the linearly congruent portions of the circulation pattern indices from the DTR time series has only a minor effect on the spatial pattern of DTR trends over the United States. Only in the south-central states and coastal Northwest do the DTR-related circulation indices consistently explain portions of the DTR trends. The south-central states and coastal Northwest also happen to be the two regions where significant trends in sunshine duration (Table 5.4) as well as strong correlations between the circulation indices and p_{sun} (Table 5.3) are found. As mentioned in the previous subsection, the observed long-term changes in the circulation, cloudiness, and the DTR are all consistent with

those expected in conjunction with the 1976/77 jump in the Pacific Decadal Oscillation which was associated with rising geopotential heights over the Pacific Northwest and falling heights over the Gulf of Mexico (Mantua et al. 1997; Higgins et al. 2000).

5.6 Summary and Discussion

In this chapter, relationships between the DTR, sunshine duration, snow cover, and the atmospheric circulation during the cold season have been investigated. The conclusions drawn from these analyses may be summarized as follows.

1. In the northern Plains and Midwest, the DTR under mostly clear skies is lower when snow is present than when the ground is snow-free, while under cloudy conditions, the presence of snow affects the DTR to a much lesser extent (Table 5.2). As a result, the correlation between the DTR and sunshine duration is also lowered when snow covers the ground (Table 5.1). In the Northeast, however, the presence of snow has only a minimal effect on the DTR.
2. Circulation patterns associated with high (low) values of the DTR in a particular region feature positive (negative) 1000-mb height anomalies centered over or near the region, with a configuration that favors the flow of relatively dry continental (moist marine) air over the area of interest (Fig. 5.3).
3. For the cold seasons (November-March) of 1965/66-1994/95, negative DTR trends, which are concentrated in the central and southern United States, prevail over positive trends, which are found primarily in the Northeast, along the Pacific coast, and over northern portions of the interior West (Fig. 5.4a). A comparison of trends based on the FSOD data (Fig. 5.7a) and trends based on data from the GHCN (Fig. 5.8a) suggests that

changes in instrumentation, station moves, and other spurious discontinuities do not contribute significantly to the DTR trends.

4. The observed negative DTR trend in the south-central United States and the positive DTR trend in the coastal Northwest appear to be partly associated with concomitant trends in cloudiness and the atmospheric circulation (Tables 5.3-5.5, Figs. 5.4b and 5.7-5.8) which may, in turn, be linked to the 1976/77 shift in the Pacific Decadal Oscillation. The observed trends in the DTR over the remainder of the country do not appear to be linearly related to changes in cloudiness, the atmospheric circulation, or snow cover extent.

Considering the nonlinearity of the relationships among the DTR, sunshine duration, and snow cover, it would be instructive to investigate changes in the DTR and snow cover extent on clear days only. A preliminary analysis with the present dataset indicates that on mostly sunny days ($p_{sun} \geq 75\%$), the DTR in the northern Plains, Midwest, and Northeast increased, while snow cover extent decreased significantly in the northern Plains and Northeast and slightly in the Midwest (not shown). This finding suggests a small positive contribution of snow cover to the DTR trends in these regions. However, in order to adequately assess the statistical significance and overall importance of this contribution, a longer period of record and a larger number of stations with the requisite data are needed.

As was pointed out by Kalkstein et al. (1996), correlations between synoptic-scale patterns and meteorological observations at the surface cannot be expected to be perfect since the same synoptic situations can result in a variety of surface conditions and vice versa. Furthermore, correlation analysis is a crude tool that reveals only simultaneous linear relationships when the causal linkages in nature may be more complex. A few nonlinearities are revealed in certain regions, for example, when composites of 1000-mb height anomalies for daily regional-mean

DTR values that are more than one standard deviation above normal are compared to composites for DTR values that are more than one standard deviation below normal (not shown). The application of other techniques such as cluster analysis in future work may shed further light on synoptic-scale patterns that favor high or low values of the DTR. Finally, the aggregation of data into regions and five-month seasons, while providing large samples for statistical analysis, may obscure certain relationships. Despite these limitations, the analysis of Section 5.4 has revealed some physically and statistically significant circulation patterns that are associated with variations in the DTR.

The fact that the analyses of Section 5.5 leave the majority of the observed cold season DTR trends unexplained implies either that the relationships between the DTR, sunshine duration, the atmospheric circulation, and snow cover extent are not adequately captured by linear analysis techniques or that factors not considered in this study contribute to the trends. Local and regional decreases in the DTR may be attributable to anthropogenic influences such as urbanization and the rise in the concentration of tropospheric aerosols and greenhouse gases. The local effects of urbanization on surface air temperature are well-documented (Cayan and Douglas 1984; Karl et al. 1988; Balling and Idso 1989; Van den Dool et al. 1993; Gallo et al. 1996, 1999). Buildings and pavement tend to retain heat for a greater length of time than undeveloped, open landscape, resulting primarily in shallow surface warming at night. The urban heat island effect is expected to be particularly noticeable in the temperature trends of stations located in areas of rapid population growth such as the desert Southwest (Cayan and Douglas 1984), which has experienced the largest trend in TD_{am} of the eight regions examined here (Table 5.4). However, since negative trends also prevail at the mainly rural stations in the GHCN dataset, it appears that factors other than urbanization contribute to the DTR decreases.

Aerosols can raise the planetary albedo and serve as condensation nuclei, thus decreasing the intensity of daytime surface heating and possibly increasing the amount of cloudiness (Charlson et al. 1992; Hansen et al. 1995; Karl et al. 1995; Dai et al. 1997). The influence of these mechanisms on local and regional DTR has yet to be investigated in detail.

Even though diurnal variations in the direct longwave radiative effect of atmospheric greenhouse gases on surface air temperature are believed to be small (Stenchikov and Robock 1995; Dai et al. 1999), the longwave radiative effects of an increase in greenhouse gases may alter nighttime boundary layer processes and, therefore, daily minimum temperatures under clear skies: the enhanced downward flux of longwave radiation from the atmospheric layer containing the increased concentrations of greenhouse gases would require a larger upward flux of longwave radiation from the earth's surface and, therefore, a warmer surface temperature. This primary effect is not expected to vary with time of day. However, the warmer surface could inhibit the formation of near-surface inversions during clear nights and thus slow the nighttime drop of surface air temperature. On the other hand, on clear days, the daily maximum temperature should be limited primarily by convective mixing with the overlying atmosphere and should therefore be largely unaffected by the radiative effects of a change in the concentration of greenhouse gases. Since water vapor is one of the greenhouse gases, an analysis of the relationship between the DTR, stability in the atmospheric boundary layer, and tropospheric water vapor under clear skies may be used in future work to assess the effect of increases in greenhouse gases on the frequency of nighttime inversions and the DTR.

TABLE 5.1 Correlations between daily anomalies of the diurnal temperature range and percent of possible sunshine during the cold season (November-March). Anomalies for 1965/66 through 1994/95 at all stations within a particular region are aggregated into a single set of station-days. For each regional aggregate, correlations are computed for all station-days (All), station-days without snow on the ground (No SOG), and station-days with a snow depth of at least 2.5 cm (SOG). The SOG-day correlation is computed only when at least 25% of all station-days within a region are days with snow on the ground. N denotes the number of stations used.

Region	*N*	*Correlation*			*% of days*	
		All	*No SOG*	*SOG*	*No SOG*	*SOG*
Northeast	13	0.39	0.41	0.35	65	35
Midwest	17	0.49	0.53	0.41	67	33
Southeast	12	0.60	0.60		97	3
Northern Plains	7	0.44	0.57	0.34	43	57
Southern Plains	3	0.59	0.62	0.48	75	25
South-Central States	5	0.69	0.69		99	1
Southwest	5	0.58	0.58		99	1
Coastal Northwest	2	0.60	0.61		97	3

TABLE 5.2 Average diurnal temperature range anomalies on clear and cloudy cold season days with (SOG) and without (No SOG) snow on the ground. A day is defined as clear (cloudy) if the day's percent of possible sunshine is greater than or equal to 90% (less than or equal to 10%). Station data for the cold seasons of 1965/66-1994/95 are grouped into regional aggregates of station-days as for Table 5.1.

Region	*No SOG*		*SOG*	
	Clear	*Cloudy*	*Clear*	*Cloudy*
Northeast	1.69	-2.01	1.50	-1.96
Midwest	2.98	-2.30	1.67	-2.17
Northern Plains	3.61	-3.81	1.26	-2.74
Southern Plains	3.92	-4.45	1.05	-4.48

TABLE 5.3 Daily correlations (×100) between time series of DTR-related 1000-mb height patterns and other variables for the cold season (November-March). Variables include the daily maximum (T_{max}), minimum (T_{min}), and range (DTR) of surface air temperature, afternoon (TD_{pm}) and morning (TD_{am}) surface-to-850-mb temperature differences, and percent of possible sunshine (p_{sun}). Correlations are based on regional time series of daily anomalies. For DTR and p_{sun} in the Northeast, Midwest, and Great Plains, correlations are shown for all days (All) and days with no snow on the ground (No SOG). The period 1958/59-1994/95 is used for all temperature variables; the period 1965/66-1994/95 is used for p_{sun}. Correlations greater than or equal to 0.08 are significant at the 5% level.

Region	*DTR*		*p_{sun}*		*TD_{pm}*	*T_{max}*	*TD_{am}*	*T_{min}*
	All	*No SOG*	*All*	*No SOG*				
Northeast	33	36	-17	-13	26	51	-26	33
Midwest	37	39	19	22	39	33	-22	15
Southeast	35		5		45	53	-12	29
Northern Plains	45	56	16	27	45	46	-41	22
Southern Plains	52	45	24	24	56	64	-28	42
South-Central	56		43		61	68	-15	34
Southwest	45		23		3	20	-42	-20
Coastal Northwest	55		54		-13	-14	-50	-54

TABLE 5.4 Regional cold season trends for 1965/66-1994/95. Variables include the diurnal temperature range (DTR), daily maximum (T_{max}) and daily minimum (T_{min}) temperatures, afternoon (TD_{pm}) and morning (TD_{am}) surface-to-850-mb temperature differences, percent of possible sunshine (p_{sun}), snow cover extent (SE), and index time series of the DTR-related circulation patterns (Circ). Units are °C (30 yrs)$^{-1}$ for all temperature variables, % (30 yrs)$^{-1}$ for p_{sun} and SE, and (standard deviation)(30 yrs)$^{-1}$ for the circulation indices. Trends significant at the 0.05 level are printed in boldface type. Trends in snow cover extent are not computed for the southern and western coastal regions.

Region	*DTR*	T_{max}	T_{min}	TD_{pm}	TD_{am}	p_{sun}	*SE*	*Circ*
Northeast	**0.7**	**1.7**	1.0	0.2	-0.4	0.9	**-10.9**	0
Midwest	0.0	**1.5**	**1.5**	-0.2	-0.4	-1.0	-4.4	0.1
Southeast	-0.6	**1.2**	**1.9**	-0.4	0.1	-5.8		-0.2
Northern Plains	-0.5	**2.5**	**3.0**	-0.1	0.6	0.1	0.2	0.1
Southern Plains	-0.4	0.8	**1.3**	-0.2	0.5	2.5	-2.0	**-0.2**
South-Central States	**-1.0**	-0.1	0.9	**-0.8**	0.2	**-8.9**		**-0.3**
Southwest	**-1.2**	0.6	**1.7**	**0.8**	**2.2**	-2.3		**0.5**
Coastal Northwest	**0.8**	0.7	-0.1	**-1.0**	**-2.1**	**6.5**		**0.2**

TABLE 5.5 Total and residual trends in regional-mean diurnal temperature range (DTR) for the cold seasons of 1965/66-1994/95. R_{circ} denotes the residual trend after the contribution from the region's DTR-related circulation pattern has been removed. R_{sun} denotes the residual trend after the contribution of percent of possible sunshine has been removed. R_{both} denotes the residual trend after the contributions of both the pattern and percent of possible sunshine have been removed. Trends significant at the 0.05 level are printed in boldface type.

Region	*Total*	R_{sun}	R_{circ}	R_{both}
Northeast	**0.7**	**0.6**	**0.7**	**0.6**
Midwest	0.0	0.1	-0.1	0.0
Southeast	-0.6	-0.1	-0.4	0.1
Northern Plains	-0.5	**-0.5**	**-0.7**	**-0.6**
Southern Plains	-0.4	**-0.8**	-0.1	**-0.5**
South-Central States	**-1.0**	-0.1	-0.4	0.0
Southwest	**-1.2**	**-0.9**	**-1.8**	**-1.4**
Coastal Northwest	**0.8**	**0.5**	**0.5**	**0.4**

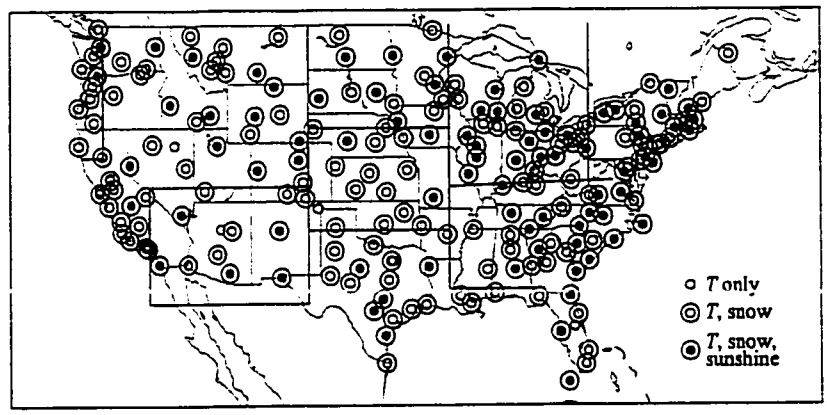

FIGURE 5.1 Map of stations and regions used in this chapter. Region boundaries are indicated by solid lines. All stations have high-quality records of daily maximum and minimum temperatures. Closed circles identify those stations with also have high-quality records of percent of possible sunshine. Concentric circles indicate the availability of a high-quality snow depth record in addition to the other data.

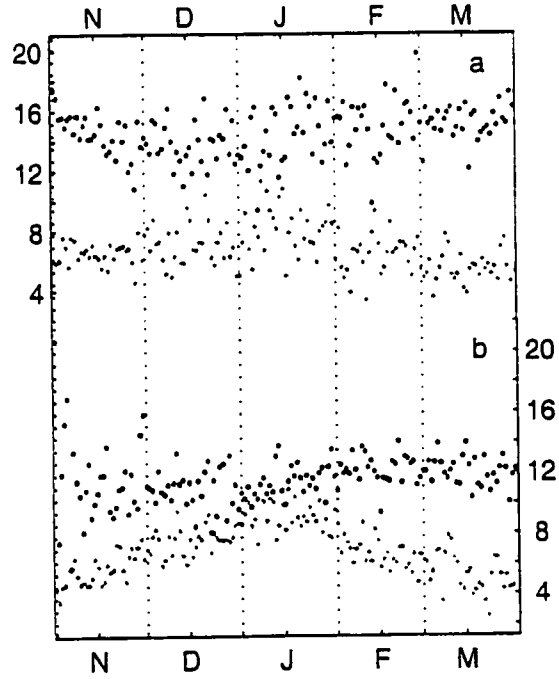

FIGURE 5.2 Average diurnal temperature range (DTR, °C) in the Northern Great Plains for clear (black) and cloudy (gray) days between November 1 and March 31 on which the ground is (a) snow-free (snow depth = 0) and (b) covered with at least 2.5 cm of snow. Days are defined as clear (cloudy) when the percent of possible sunshine is at least 90% (10% or less). Days between November 1 and March 31 are plotted on the x-axis, the DTR on the y-axis. Each dot represents an average over 7 stations and the period 1965/66-1994/95 for a particular calendar date.

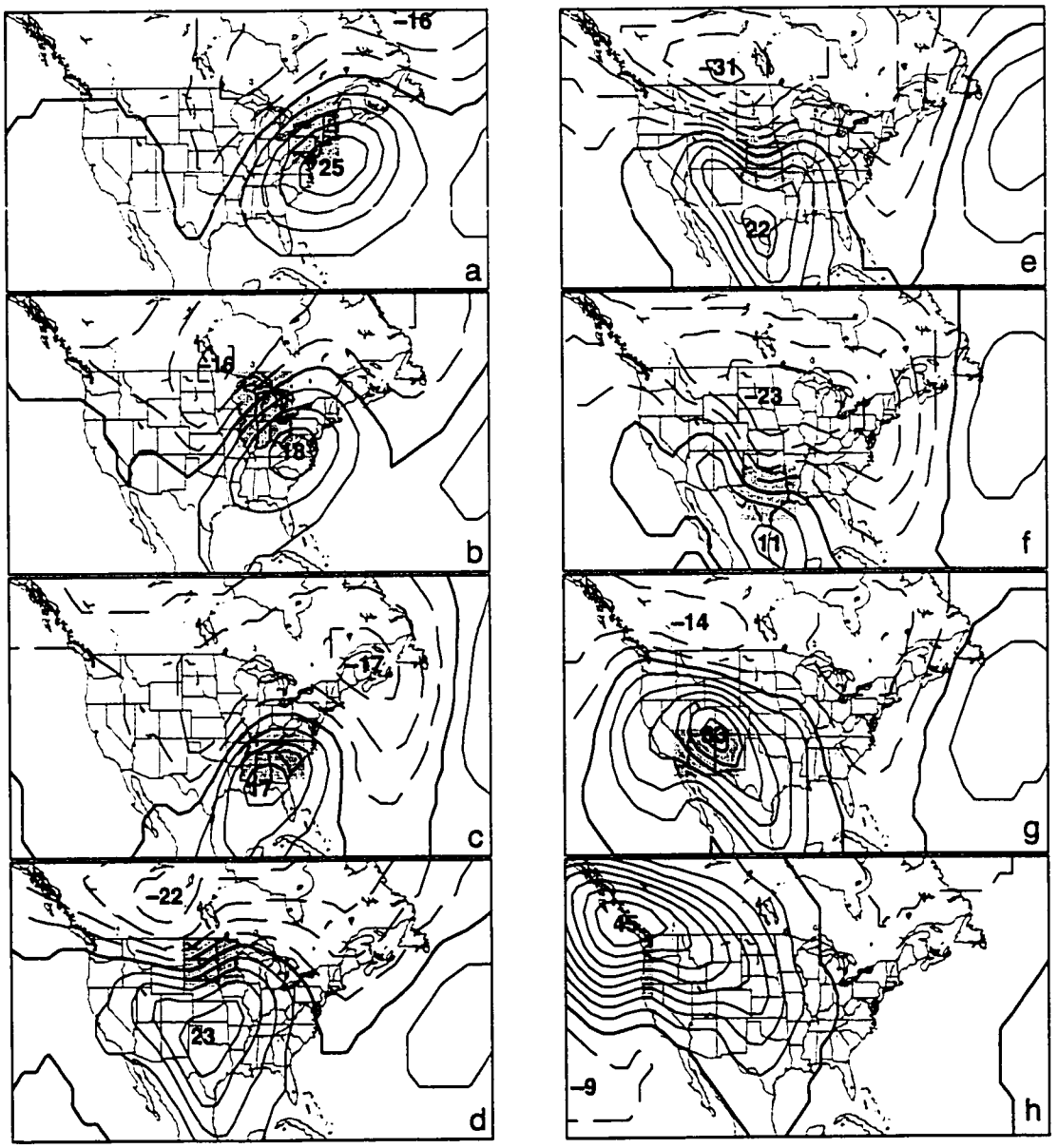

FIGURE 5.3 DTR-related regression patterns of 1000-mb geopotential height anomalies for eight regions. (a) Northeast, (b) Midwest, (c) Southeast, (d) northern Plains, (e) southern Plains, (f) central South, (g) Southwest, and (h) coastal Northwest. Values are typical for a one-standard deviation positive daily DTR anomaly during November - March. The contour interval is 5 m. Solid contours indicate positive height anomalies, dashed contours indicate negative anomalies, and the zero contour is thickened. In each panel, the pattern is related to the diurnal temperature range of the area shaded in gray.

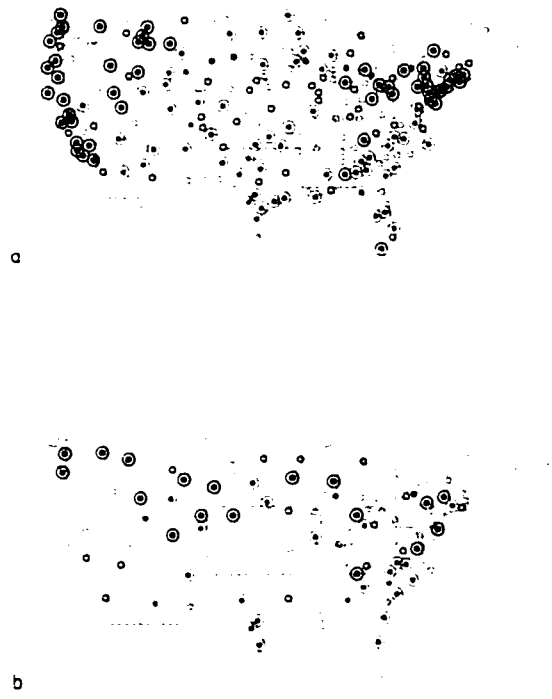

FIGURE 5.4 Station trends of (a) the diurnal temperature range and (b) percent of possible sunshine for the cold seasons of 1965/66-1994/95. Trends significant at the 5% (10%) level are marked with concentric (closed) circles. Trends not significant at the 10% level are marked with open circles. Positive trends are shown in black, negative trends in gray.

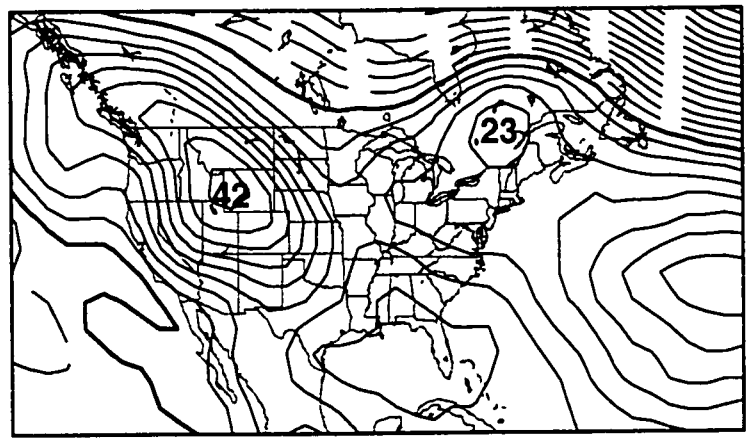

FIGURE 5.5 Trends in 1000-mb geopotential height (m (30 yrs)$^{-1}$) in the domain 20°N - 60°N, 40°W - 140°W for the cold seasons of 1965/66-1994/95. The contour interval is 10 m (30 yrs)$^{-1}$. Solid contours indicate positive trends; dashed contours indicate negative trends, and the zero contour is thickened.

FIGURE 5.6 Contributions of DTR-related atmospheric circulation patterns to station trends of the diurnal temperature range. A contribution to a station's DTR trend is based on a circulation index computed from 1000-mb heights within a (a) 5°-by-5°, (b) 10°-by-10°, and (c) 15°-by-15° latitude/longitude box centered on the station. Two concentric circles represent a 30-year trend that exceeds 5% of the station's mean cold season DTR; a closed circle represents a trend that exceeds 1% of the station's mean DTR; all smaller trends are marked by open circles. Positive trends are shown in black, negative trends in gray.

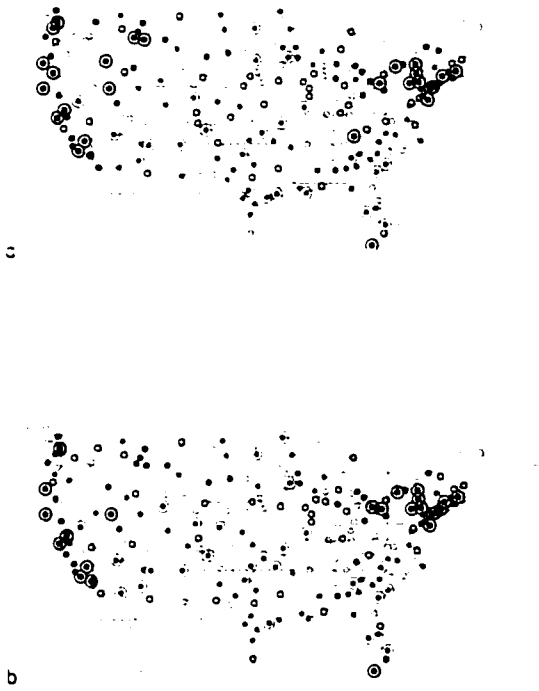

FIGURE 5.7 (a) Diurnal temperature range (DTR) trends for the cold seasons of 1965/66-1994/95 and (b) residual DTR trends following the removal of contributions from DTR-related circulation patterns, based on First Order Summary of the Day data. Two concentric circles represent a 30-year trend that exceeds 10% of the station's mean cold season DTR; a closed circle represents a trend that exceeds 5% of the station's mean DTR; all smaller trends are marked by open circles. Positive trends are shown in black, negative trends in gray.

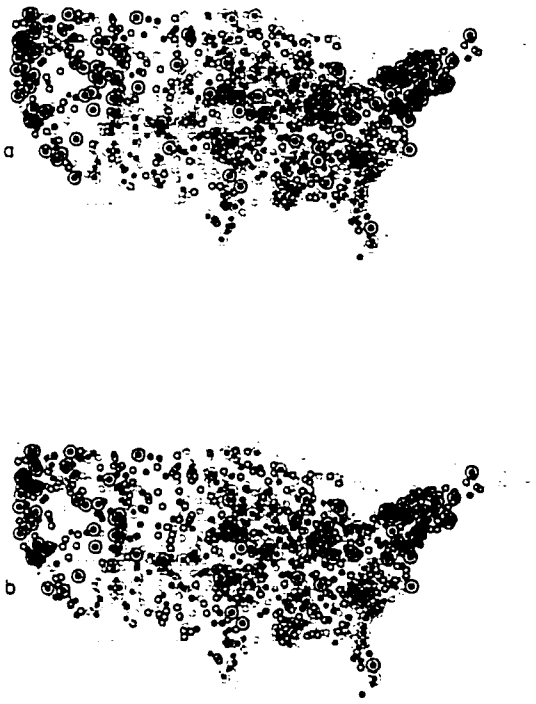

FIGURE 5.8 Diurnal temperature range trends based on data from the Global Historical Climatology Network, cold seasons 1965/66-1994/95. (a) Total 30-year trends; (b) residual trends following the removal of contributions from DTR-related circulation patterns. The scale and plotting conventions are the same as in Figure 5.7.

CHAPTER 6

Concluding Remarks

This work has presented several empirical analyses of the relationships between the daily maximum, minimum, and range of surface air temperature and other climate variables. In agreement with the findings of previous studies, the results show that by altering the net radiative, sensible, and latent heat fluxes at the surface, cloudiness and land surface conditions affect daily maximum temperature more strongly than daily minimum temperature and thereby directly influence the diurnal temperature range. Throughout the year, the highest values of the DTR are associated with a dry, bare soil under clear skies. The presence of wet soil or vegetation during summer and snow cover during winter can inhibit surface heating during the day and thus lower the DTR, particularly when insolation is strong. The effects of soil moisture and vegetation tend to be strongest in the southeastern United States, while the impact of snow cover is most important in the northern Plains.

Since it strongly controls the distribution of clouds, the atmospheric circulation also has a significant impact on the DTR. Regressions of daily 1000-mb height anomalies onto regional-mean time series of the cold season DTR indicate that anomalous anticyclonic flow over a region favors a relatively high DTR, while cyclonic flow favors a low DTR. Even though results of this regression analysis are presented only for the cold season months of November-March, similar results have been obtained for the warm season (May-September).

The motivation for this study was to improve our ability to interpret trends in the DTR. The knowledge gained from analyzing the various factors that affect the DTR is applied to 30-year trends in the DTR for the cold seasons of 1965/66-1994/95. For this period of record, decreases in the DTR prevail over increases across the United States. However, areas of significant DTR

increases are found over the Northeast, along the Pacific Coast, and in parts of the interior West. Even though negative DTR trends also prevail during the warm season, the warm season trends for 1966-1995 have been found to be smaller and less spatially coherent than the cold season trends in most locations (Fig. 6.1) and have therefore not been further analyzed.

During the cold season, changes in cloudiness contribute significantly to the decreases in the DTR over the south-central and southeastern states as well as to the DTR increase in the coastal Northwest. The trends in the DTR and cloudiness over the south-central states and coastal Northwest are physically consistent with changes in the 1000-mb height field which may, in turn, be related to the 1976/77 jump in the Pacific Decadal Oscillation. Trends in the atmospheric circulation, however, cannot account for the prevalence of negative trends in the DTR. For the period of study, none of the DTR trends are found to be significantly related to changes in snow cover extent. The results on trends in the First Summary of the Day dataset should be viewed with some caution since these data have not been corrected for changes in instrumentation, station moves, and other extraneous effects. However, a repetition of some of the analyses using monthly mean data from the Global Historical Climatology Network (GHCN) yields very similar results.

Provided that homogeneity-adjusted daily observations from foreign countries can be obtained, I plan to extend this work to other parts of the globe. Both the annual march of the DTR at locations outside the United States and the factors contributing to the DTR trends at those locations during both cold and warm seasons are of interest. In addition, the GHCN metadata on population and local landscape may assist in explaining some aspects of the small-scale spatial variability of both averages and trends in the DTR.

Future work on the association between soil moisture and the DTR should make use of the daily observations of soil moisture and other meteorological variables in the World Soil Moisture Databank (Robock et al. 2000). During the course of this study, attempts were made to examine

the relationship between vegetation and the DTR using the Normalized Difference Vegetation Index (NDVI). However, as mentioned in Section 4.3, various shortcomings of the NDVI dataset limit its utility for such purposes. An improvement of the NDVI or an expansion of land-based observations of phenological events would be of great value to researchers studying the relationship between vegetation and climate.

Other future work should include an examination of the association between tropospheric water vapor content, the DTR, and the frequency of nighttime inversions under clear skies using estimates of low-level or column water vapor based on satellite or radiosonde measurements. Such an analysis may shed light on the potential impact of increases in greenhouse gases on the DTR. The local radiative effects of tropospheric aerosols on the DTR have also yet to be explored in detail. An investigation of these effects may utilize long-term records of horizontal visibility as a proxy for the concentration of particulates in the atmospheric boundary layer. Finally, experiments with a coupled land-atmosphere-ocean model in which selected variables, such as total cloud amount, can be held fixed may further illuminate all of these interrelationships. A more complete interpretation of the trends in the DTR hinges upon the findings of all of these proposed studies.

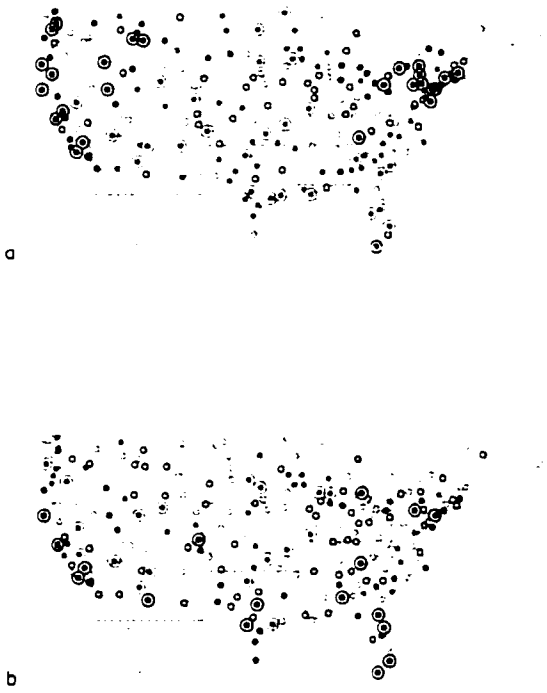

FIGURE 6.1 Trends of the diurnal temperature range at First Order Summary of the Day stations for (a) November-March 1965/66-1994/95 and (b) May-September 1966-1995. Two concentric circles represent a 30-year trend that exceeds 10% of the station's mean DTR for the season; a closed circle represents a trend that exceeds 5% of the station's mean DTR; all smaller trends are marked by open circles. Positive trends are shown in black, negative trends in gray.

BIBLIOGRAPHY

Alley, W. M., 1984: The Palmer drought severity index: limitations and assumptions. *J. Climate Appl. Meteor.*, **23**, 1100-1109.

Angell, J. K., 1990: Variation in United States cloudiness and sunshine duration between 1950 and the drought year of 1988. *J. Climate*, **3**, 296-308.

_____ and J. Korshover, 1987: Variability in United States cloudiness and its relation to El Niño. *J. Climate Appl. Meteor.*, **26**, 580-584.

Balling, R. C. Jr., and S. B. Idso, 1989: Historical temperature trends in the United States and the effect of urban population growth. *J. Geophys. Res.*, **94**, 3359-3363.

Batjes, N. H., 1996: Development of a world data set of soil water retention properties using pedotransfer rules. *Geoderma*, **71**, 31-52.

Bravar, L., and M. L. Kavvas, 1991: On the physics of drought. I. A conceptual framework. *J. Hydrol.*, **129**, 281-297.

Bristow, K. L., and G. S. Campbell, 1984: On the relationship between incoming solar radiation and daily maximum and minimum temperature. *Agric. For. Meteor.*, **31**, 159-166.

Brown, R. D., M. G. Hughes, and D. A. Robinson, 1995: Characterizing the long-term variability of snow-cover over the interior of North America. *Ann. Glaciol.*, **21**, 45-50.

Brubaker, K. L., D. Entekhabi, and P. S. Eagleson, 1993: Estimation of continental precipitation recycling. *J. Climate*, **6**, 1077-1089.

Budyko, M. I., 1956: *Heat Balance of the Earth's Surface*. Gidrometeozidat, Leningrad, 255 pp.

Buffo, J., L. Fritschen, and J. Murphy, 1972: Direct Solar Radiation on Various Slopes from 0 to 60 North Latitude. USDA Forest Service Research Paper PNW-142. [Available from National

Forest Service, PO Box 96090, 14th and Independence Avenue, SW, Washington. DC 20090-6090.]

Campbell, G. G., and T. H. Vonder Haar, 1997: Comparison of surface temperature minimum and maximum and satellite measured cloudiness and radiation. *J. Geophys. Res.*, **102**, 16639-16645.

Cao, H. X., J. F. B. Mitchell, J. R. Lavery, 1992: Simulated diurnal range and variability of surface temperature in a global climate model for present and doubled CO_2 climates. *J. Climate*, **5**, 920-943.

Cayan, D. R., and A. V. Douglas, 1984: Urban influences on surface temperatures in the southwestern United States during recent decades. *J. Climate Appl. Meteor.*, **23**, 1520-1530.

Cerveny, R. S., and R. C. Balling, Jr., 1992: The impact of snow cover on diurnal temperature range. *Geophys. Res. Lett.*, **19**, 797-800.

Chang, F.-C., and J. M. Wallace, 1987: Meteorological conditions during heat waves and droughts in the United States Great Plains. *Mon. Wea. Rev.*, **115**, 1253-1269.

Charlson, R. J., S. E. Schwartz, J. M. Hales, R. D. Cess, J. A. Coakley, Jr., J. E. Hansen, and D. J. Hofmann, 1992: Climate forcing by anthropogenic aerosols. *Science*, **255**, 423-430.

CNC (Committee for Natural Classification, Chinese Academy of Sciences), 1959: *Climate Classification of China*. Science Press, 456 pp.

Croke, M., R. D. Cess, and S. Hameed, 1999: Regional cloud cover change associated with global climate change: case studies for three regions of the United States. *J. Climate*, **12**, 2128-2134.

Crutcher, H. L., 1978: Temperature and Precipitation Correlations Within the United States. NOAA Technical Report EDS 26, NTIS Report No. NOAATREDS26; NOAA78022101, 42 pp.

Dai, A., A. D. Del Genio, and I. Fung, 1997: Clouds, precipitation, and temperature range. *Nature*, **386**, 6651-6666.

_____, K. E. Trenberth, and T. R. Karl, 1999: Effects of clouds, soil moisture, precipitation and water vapor on diurnal temperature range. *J. Climate*, **12**, 2451-2473.

Davis, R. E., and D. R. Walker, 1992: An upper-air synoptic climatology of the western United States. *J. Climate*, **5**, 1449-1467.

Delworth, T. L., and S. Manabe, 1988: Influence of potential evaporation on the variabilities of simulated soil wetness and climate. *J. Climate*, **1**, 523-547.

Dewey, K., 1977: Daily maximum and minimum temperature forecasts and the influence of snow cover. *Mon. Wea. Rev.*, **105**, 1594-1597.

Diaz, H. F., 1983: Drought in the United States – Some aspects of major dry and wet periods in the contiguous United States, 1895-1981. *J. Climate Appl. Meteor.*, **22**, 3-16.

Dirmeyer, P. A., 1994: Vegetation stress as a feedback mechanism in midlatitude drought. *J. Climate*, **7**, 1463-1483.

Dorman, J. L., and P. J. Sellers, 1989: A global climatology of albedo, roughness length, and stomatal resistance for atmospheric general circulation models as represented by the Simple Biosphere Model (SiB). *J. Appl. Meteor.*, **28**, 833-855.

Easterling, D. R., and co-authors, 1997: Maximum and minimum temperature trends for the globe. *Science*, **277**, 164-167.

Eastern North America Phenology Network, cited 1999: 30-year normal first-leaf date map (three-plant average). [Available online from http://www.uwm.edu/~mds/enanet.html.]

Elliott, W. P., and J. K. Angell, 1997: Variations of cloudiness, precipitable water, and relative humidity over the United States: 1973-1993. *Geophys. Res. Lett.*, **24**, 41-44.

Eltahir, E. A. B., and R. L. Bras, 1996: Precipitation recycling. *Rev. Geophys.*, **34**, 367-378.

Entekhabi, D., I. Rodriguez-Iturbe, R. L. Bras, 1992: Variability in large-scale water balance with land surface-atmosphere interaction. *J. Climate*, **5**, 798-814.

Fennessy, M. J., and J. Shukla, 1999: Impact of initial soil wetness on seasonal atmospheric prediction. *J. Climate*, **12**, 3167-3180.

France, L., cited 2000: Summary of the Day – First Order – TD-3210. Asheville, NC: National Climatic Data Center. [Available online from http://www.ncdc.noaa.gov.]

Gaffen, D. J., and R. J. Ross, 1999: Climatology and trends of U.S. surface humidity and temperature. *J. Climate*, **12**, 811-828.

Gallo, K. P., D. R. Easterling, and T. C. Peterson, 1996: The influence of land use/land cover on climatological values of the diurnal temperature range. *J. Climate*, **9**, 2941-2944.

_____, T. W. Owen, and D. R. Easterling, 1999: Temperature trends of the U.S. Historical Climatology Network based on satellite-designated land use/land cover. *J. Climate*, **12**, 1344-1348.

Gardner, B. R., B. L. Blad, and D. G. Watts, 1981: Plant and air temperatures in differentially irrigated corn. *Agric. Meteor.*, **25**, 207-217.

Georgakakos, K. P., D.-H. Bae, and D. R. Cayan, 1995: Hydroclimatology of continental watersheds. 1. Temporal Analysis. *Water Resour. Res.*, **31**, 655-675.

Groisman, P. Y., T. R. Karl, R. W. Knight, and G. L. Stenchikov, 1994: Changes of snow cover, temperature, and radiative heat balance over the Northern Hemisphere. *J. Climate*, **7**, 1633-1656.

_____, E. L. Genikhovich, and P. M. Zhai, 1996: "Overall" cloud and snow cover effects on internal climate variables: the use of clear-sky climatology. *Bull. Amer. Meteor. Soc.*, **77**, 2065-2075.

_____, R. S. Bradley, and B. Sun, 2000: The relationship of cloud cover to near-surface temperature and humidity: comparison of GCM simulations with empirical data. *J. Climate*, **13**, 1858-1878.

Hameed, S., and I. Pittalwala, 1989: An investigation of the instrumental effects on the historical sunshine records for the United States. *J. Climate*, **2**, 101-104.

Hansen, J., M. Sato, and R. Ruedy, 1995: Long-term changes of the diurnal temperature cycle: implications about mechanisms of global climate change. *Atmos. Res.*, **37**, 175-209.

Higgins, R. W., A. Leetmaa, Y. Xue, and A. Barnston, 2000: Dominant factors influencing the seasonal predictability of United States precipitation and surface air temperature. *J. Climate*, in press.

Hollinger, S. E., and S. A. Isard, 1994: A soil moisture climatology of Illinois. *J. Climate*, **7**, 822-833.

Horton, B., 1995: Geographical distribution of changes in maximum and minimum temperatures. *Atmos. Res.*, **37**, 101-117.

Huang, J., and H. M. Van den Dool, 1993: Monthly precipitation-temperature relations and temperature predictions over the United States. *J. Climate*, **6**, 1111-1132.

_____, _____, and K. P. Georgakakos, 1996: Analysis of model-calculated soil moisture over the United States (1931-1993) and applications to long-range temperature forecasts. *J. Climate*, **9**, 1350-1362.

Hughes, M. G., and D. A. Robinson, 1996: Historical snow cover variability in the Great Plains region of the USA: 1910 through to 1993. *Int. J. Climatol.*, **16**, 1005-1018.

Hurrell, J. W., 1995: Decadal trends in the North Atlantic Oscillation: regional temperatures and precipitation. *Science*, **269**, 676-679.

Kalkstein, L. S., M. C. Nichols, C. D. Barthel, and J. S. Greene, 1996: A new synoptic classification: application to air-mass analysis. *Int. J. Climatol.*, **16**, 983-1004.

Kalnay, E., M. Kanamitsu, R. Kistler, W. Collins, D. Deaven, L. Gandin, M. Iredell, S. Saha, G. White, J. Woolen, Y. Zhu, M. Chelliah, W. Ebisuzaki, W. Higgins, J. Janowiak, K. C. Mo, C. Ropelewski, J. Wang, A. Leetmaa, R. Reynolds, R. Jenne, D. Joseph, 1996: The NCEP/NCAR 40-year Reanalysis Project. *Bull. Amer. Meteor. Soc.*, **77**, 437-471.

Kane, R. P., and D. Gobbi, 1995: Interannual variability of United States sunshine and cloudiness. *Ann. Geophys.*, **13**, 660-665.

Karl, T. R., 1986: Relationships Between Some Moisture Parameters and Subsequent Seasonal and Monthly Mean Temperature in the United States. Programme on Long-Range Forecasting Res. Rep. Ser., No. 6, WMO/TDD-No. 87, 2, 661-670. [Available from WMO; Office for Information and Public Affairs; 41, Avenue Giuseppe-Motta; 1211 Geneva 2 / Switzerland; PubSales@gateway.wmo.ch.]

_____ and R. G. Quayle, 1981: The 1980 heat wave and drought in historical perspective. *Mon. Wea. Rev.*, **109**, 2055-2077.

_____ and P. M. Steurer, 1990: Increased cloudiness in the United States during the first half of the Twentieth Century: fact or fiction? *Geophys. Res. Lett.*, **17**, 1925-1928.

_____, G. Kukla, and J. Gavin, 1984: Decreasing diurnal temperature range in the United States and Canada from 1941 through 1980. *J. Climate Appl. Meteor.*, **23**, 1489-1504.

_____, _____, and _____, 1987: Recent temperature changes during overcast and clear skies in the United States. *J. Climate Appl. Meteor.*, **26**, 698-710.

_____, H. F. Diaz, and G. Kukla, 1988: Urbanization: its detection and effect in the United States climate record. *J. Climate*, **1**, 1099-1123.

_____, P. Y. Groisman, R. W. Knight, and R. R. Heim, Jr., 1993a: Recent variations of snow cover and snowfall in North America and their relation to precipitation and temperature variations. *J. Climate*, **6**, 1327-1344.

_____, P. D. Jones, R. W. Knight, G. Kukla, N. Plummer, V. Razuvaev, K. P. Gallo, J. Lindseay, R. J. Charlson, and T. C. Peterson, 1993b: A new perspective on recent global warming: asymmetric trends of maximum and minimum temperature. *Bull. Amer. Meteor. Soc.*, **74**, 1007-1023.

_____, R. W. Knight, G. Kukla, and J. Gavin, 1995: Evidence for radiative effects of anthropogenic sulfate aerosols in the observed climate record. *Aerosol Forcing and Climate*, R. J. Charlson and J. Heintzenberg, Eds., John Wiley & Sons, 363-382.

Kaufmann, M. R., 1984: A canopy model (RM-CwW) for determining transpiration of subalpine forests. Part II: consumptive water use in two watersheds. *Can. J. For. Res.*, **14**, 227-232.

Kimball, J. S., S. W. Running, and R. Nemani, 1997: An improved method for estimating surface humidity from daily minimum temperature. *Agric. For. Meteor.*, **85**, 87-98.

Knappenberger, P., P. Michaels, and P. Schwartzman, 1996: Observed changes in diurnal temperature and dewpoint cycles across the United States. *Geophys. Res. Lett.*, **23**, 2637-2640.

Koster, R. D., and M. J. Suarez, 1996: The influence of land surface moisture retention on precipitation statistics. *J. Climate*, **9**, 2551-2567.

Kukla, G., J. Gavin, M. Schlesinger, and T. Karl, 1995: Comparison of observed seasonal temperature maxima, minima, and diurnal range in North America with simulations from three global climate models. *Atmos. Res.*, **37**, 267-275.

Lanzante, J. R., 1996: Resistant, robust, and non-parametric techniques for the analysis of climate data: theory and applications, including applications to historical radiosonde station data. *Int. J. Climatol.*, **16**, 1197-1126.

Leathers, D. J., B. Yarnal, and M. A. Palecki, 1991: The Pacific/North American teleconnection pattern and United States climate. Part I: regional temperature and precipitation associations. *J. Climate*, **4**, 517-528.

_____, T. L. Mote, K. C. Kuivinen, S. McFeeters, and D. R. Kluck, 1993: Temporal characteristics of USA snowfall 1945-46 to 1984-85. *Int. J. Climatol.*, **13**, 65-76.

_____, A. W. Ellis, and D. A. Robinson, 1995: Characteristics of temperature depression associated with snow cover across the Northeast United States. *J. Appl. Meteor.*, **34**, 381-390.

_____, M. A. Palecki, D. A. Robinson, and K. F. Dewey, 1998: Climatology of the diurnal temperature range annual cycle in the United States. *Climate Res.*, **9**, 197-211.

Leith, C. E., 1973: The standard error of time-average estimates of climatic means. *J. Appl. Meteor.*, **12**, 1066-1069.

Lettenmaier, D. P., E. F. Wood, and J. R. Wallis, 1994: Hydro-climatological trends in the contiguous United States: 1948-88. *J. Climate*, **7**, 586-607.

Madden, R. A., and J. Williams, 1978: The correlation between temperature and precipitation in the United States and Europe. *Mon. Wea. Rev.*, **106**, 142-147.

Manabe, S., J. Smagorinsky, and R. F. Strickler, 1965: Simulated climatology of a general circulation model with a hydrologic cycle. *Mon. Wea. Rev.*, **93**, 769-798.

Mantua, N. J., S. R. Hare, Y. Zhang, J. M. Wallace, and R. C. Francis, 1997: A Pacific interdecadal climate oscillation with impacts on salmon production. *Bull. Amer. Meteor. Soc.*, **78**, 1069-1079.

McCabe, G. J. Jr., and D. R. Legates, 1995: Relationships between 700-mb height anomalies and 1 April snowpack accumulations in the western USA. *Int. J. Climatol.*, **15**, 517-530.

McNab, A. L., 1989: Climate and drought. *EOS*, **70**, 873, 882-883.

Mearns, L. O., F. Giorgi, L. McDaniel, and C. Shields, 1995: Analysis of variability and diurnal range of daily temperature in a nested regional climate model: comparison with observations and doubled CO_2 results. *Climate Dyn.*, **11**, 193-209.

Namias, J., 1960: Factors in the Initiation, Perpetuation and Termination of Drought. Extract of Publ. No. 51, International Association of Hydrological Sciences (IAHS) Commission of Surface Waters. [Available from IAHS Press, Institute of Hydrology, Wallingford, Oxfordshire OX10 8BB, UK.]

_____, 1983: Some causes of United States drought. *J. Climate Appl. Meteor.*, **22**, 30-39.

National Climatic Data Center, cited 1998: Time bias corrected divisional temperature-precipitation-drought index: TD-9640 tape documentation. Asheville, NC: National Climatic Data Center. [Available online from ftp.ncdc.noaa.gov.]

Oliver, S. A., H. R. Oliver, J. S. Wallace, and A. M. Roberts, 1987: Soil heat flux and temperature variation with vegetation, soil type and climate. *Agric. For. Meteor.*, **39**, 257-269.

Palmer, W. M., 1965: Meteorological Drought. Res. Pap. No. 45, U.S. Weather Bureau, 58 pp. [Available from NOAA Library and Information Services Division, Washington, DC 20852.]

Penman, H. L., 1948: Natural evaporation from open water, bare soil, and grass. *Proc. Roy. Soc., London*, **193A**, 120-145.

Peterson, T. C., and R. S. Vose, 1997: An overview of the Global Historical Climatology Network Temperature Database. *Bull. Amer. Meteor. Soc.*, **78**, 2837-2849.

Plantico, M. S., T. R. Karl, G. Kukla, and J. Gavin, 1990: Is recent climate change across the United States related to rising levels of anthropogenic greenhouse gases? *J. Geophys. Res.*, **95**, 16617-16637.

Priestley, C. H. B., and R. J. Taylor, 1972: The assessment of surface heat flux and evaporation using large scale parameters. *Mon. Wea. Rev.*, **106**, 81-92.

Przybylak, R., 2000: Diurnal temperature range in the Arctic and its relation to hemispheric circulation patterns. *Int. J. Climatol.*, **20**, 231-253.

Radersma, S., and N. de Reider, 1996: Computed evapotranspiration of annual and perennial crops at different temporal and spatial scales using published parameter values. *Agric. Water Management*, **31**, 17-34.

Razuvaev, R. N., E. G. Apasova, and R. A. Martuganov, 1995: Variations in the diurnal temperature range in the European region of the former USSR during the cold season. *Atmos. Res.*, **37**, 45-51.

Reed, B. C., J. F. Brown, D. Vanderzee, T. R. Loveland, J. W. Merchant, and D. O. Ohlen, 1994: Measuring phenological variability from satellite imagery. *J. Veg. Sci.*, **5**, 703-714.

Rind, D., 1982: The influence of ground moisture conditions in North America on summer climate as modeled in the GISS GCM. *Mon. Wea. Rev.*, **110**, 1488-1494.

_____, R. Goldberg, and R. Ruedy, 1989: Change in climate variability in the 21st century. *Climatic Change*, **14**, 5-37.

Robinson, D. A., D. J. Leathers, M. A. Palecki, K. F. Dewey, 1995: Some observations on climate variability as seen in daily temperature structure. *Atmos. Res.*, **37**, 19-31.

Robinson, P. J., 1992: Trends in the relationship between monthly and daily temperatures across the United States. *Phys. Geogr.*, **13**, 191-205.

Robock, A., 1980: The seasonal cycle of snow cover, sea ice and surface albedo. *Mon. Wea. Rev.*, **108**, 267-285.

_____, K. Y. Vinnikov, G. Srinivasan, J. K. Entin, S. E. Hollinger, N. A. Speranskaya, S. Liu, and A. Namkhai, 2000: The Global Soil Moisture Data Bank. *Bull. Amer. Meteor. Soc.*, **81**, 1281-1300.

Ruschy, D. L., D. G. Baker, and R. J. Skaggs, 1991: Seasonal variation in daily temperature ranges. *J. Climate*, **4**, 1211-1216.

Saltzman, B., and J. A. Pollack, 1977: Sensitivity of the diurnal surface temperature range to changes in physical parameters. *J. Appl. Meteor.*, **16**, 614-619.

Schwartz, M. D., 1990: Detecting the onset of spring: a possible application of phenological models. *Climate Res.*, **1**, 23-29.

_____, 1992: Phenology and springtime surface-layer change. *Mon. Wea. Rev.*, **120**, 2570-2578.

_____, 1996: Examining the spring discontinuity in daily temperature ranges. *J. Climate*, **9**, 803-808.

_____ and T. R. Karl, 1990: Spring phenology: nature's experiment to detect the effect of 'green-up' on surface maximum temperatures. *Mon. Wea. Rev.*, **118**, 883-890.

_____ and B. R. Skeeter, 1994: Linking air mass analysis to daily and monthly mid-tropospheric flow patterns. *Int. J. Climatol.*, **14**, 439-464.

_____ and B. C. Reed, 1999: Surface phenology and satellite sensor-derived onset of greenness: an initial comparison. *Int. J. Remote Sens.*, **20**, 3451-3457.

Shukla, H., and Y. Mintz, 1982: The influence of land surface evapotranspiration on the earth's climate. *Science*, **215**, 1498-1501.

Skeeter, B. R., and A. J. Park, 1985: Synoptic control of regional temperature trends in the coterminous United States between 1949 and 1981. *Phys. Geogr.*, **6**, 69-84.

Somayao, C. R., E. T. Kanemasu, T. W. Brakke, 1980: Using leaf temperature to assess evapotranspiration and advection. *Agric. Meteor.*, **22**, 153-166.

Stamm, J. F., E. F. Wood, and D. P. Lettenmaier, 1994: Sensitivity of a GCM simulation of global climate to the representation of land-surface hydrology. *J. Climate*, **7**, 1218-1239.

Stenchikov, G. L., and A. Robock, 1995: Diurnal asymmetry of climatic response to increased CO_2 and aerosols: forcings and feedbacks. *J. Geophys. Res.*, **100**, 26211-26227.

Sun, B., P. Y. Groisman, R. S. Bradley, and F. T. Keimig, 2000: Temporal changes in the observed relationship between cloud cover and surface air temperature. *J. Climate*, in press.

Swift, L. W. Jr., 1976: Algorithm for solar radiation on mountain slopes. *Water Resour. Res.*, **12**, 108-112.

Thompson, D. W. J., and J. M. Wallace, 1998: The Arctic Oscillation signature in the wintertime geopotential height and temperature fields. *Geophys. Res. Lett.*, **25**, 1297-1300.

_____ and _____, 2000: Annular modes in the extratropical circulation. Part I: month-to-month variability. *J. Climate*, **13**, 1000-1016.

Travis, D. J., and S. A. Changnon, 1997: Evidence of jet contrail influences on regional-scale diurnal temperature range. *J. Wea. Mod.*, **29**, 74-83.

Trenberth, K. E., 1999: Atmospheric moisture recycling: role of advection and local evaporation. *J. Climate*, **12**, 1368-1381.

Van den Dool, H. M., E. A. O'Lenic, and W. H. Klein, 1993: Consistency check for trends in surface temperature and upper-air circulation: 1950-1992. *J. Climate*, **6**, 2288-2297.

Verdecchia, M., G. Visconti, F. Giorgi, and M. R. Marinucci, 1994: Diurnal temperature range for a doubled carbon dioxide concentration experiment: analysis of possible physical mechanisms. *Geophys. Res. Lett.*, **21**, 1527-1530.

Wagner, A. J., 1973: The influence of average snow depth on monthly mean temperature anomaly. *Mon. Wea. Rev.*, **101**, 624-626.

Wallace, J. M., Y. Zhang, and L. Bajuk, 1996: Interpretation of interdecadal trends in Northern Hemisphere surface air temperature. *J. Climate*, **9**, 249-259.

Walsh, J. E., W. H. Jasperson, and B. Ross, 1985: Influence of snow cover and soil moisture on monthly air temperatures. *Mon. Wea. Rev.*, **113**, 756-768.

Warren, S., C. Hahn, J. London, R. Chervin, and R. Jenne, 1986: Global Distribution of Total Cloud Cover and Cloud Type Amounts Over Land. NCAR Tech. Note NCAR/TN-273+STR and DOE Tech. Rep. DOE/ER/60085-H1. U.S. Department of Energy, Carbon Dioxide Research Division, Washington, DC, 29 pp. [NTIS #PB 87 006903/AS; available as numeric data package NDP-026 from Carbon Dioxide Information Analysis Center, Oak Ridge National Laboratory, P.O. Box 2008, Oak Ridge, TN 37831-6050; (423) 574-3645.]

Williams, K. R. S., 1992: Correlations between Palmer drought indices and various measures of air temperature in the climatic zones of the United States. *Phys. Geogr.*, **13**, 349-367.

Xue, Y., M. J. Fennessy, and P. J. Sellers, 1996: The impact of vegetation properties on U.S. summer weather prediction. *J. Geophys. Res.*, **101**, 7419-7430.

Yang, R., M. J. Fennessy, and J. Shukla, 1994: The influence of initial soil wetness on medium-range surface weather forecasts. *Mon. Wea. Rev.*, **122**, 471-483.

Yeh, T. C., R. T. Wetherald, and S. Manabe, 1984: The effect of soil moisture on the short-term climate and hydrology change – a numerical experiment. *Mon. Wea. Rev.*, **112**, 474-490.

Zhao, W., and M. A. Khalil, 1993: The relationship between precipitation and temperature over the contiguous United States. *J. Climate*, **6**, 1232-1236.

VITA

I was born on October 5, 1972, in Karlsruhe, Germany. After moving to the United States with my family in 1987, I graduated as valedictorian from Poudre High School in Fort Collins, Colorado, in 1991. In 1994, I received a Bachelor of Science in Applied Mathematics with a concentration in Geology and Geophysics from Yale University in New Haven, Connecticut. From 1994 to 2000, I have been a graduate student and research assistant in Atmospheric Sciences at the University of Washington in Seattle.